nature communications

Article

https://doi.org/10.1038/s41467-024-54892-w

Thioredoxin 1 moonlights as a chaperone for an interbacterial ADP-ribosyltransferase toxin

Received: 19 March 2024

Accepted: 22 November 2024

Published online: 29 November 2024

Check for updates

Baptiste Dumont[1,5], Laurent Terradot[2], Eric Cascales[3], Laurence Van Melderen[1] ✉ & Dukas Jurėnas[1,4] ✉

Formation and breakage of disulfide bridges strongly impacts folding and activity of proteins. Thioredoxin 1 (TrxA) is a small, conserved enzyme that reduces disulfide bonds in the bacterial cytosol. In this study, we provide an example of the emergence of a chaperone role for TrxA, which is independent of redox catalysis. We show that the activity of the secreted bacterial ADP-ribosyltransferase (ART) toxin TreX, which does not contain any cysteines, is dependent on TrxA. TreX binds to the reduced form of TrxA via its carboxy-terminal extension to form a soluble and active complex. Structural studies revealed that TreX-like toxins are homologous to Scabin-like ART toxins which possess cysteine residues and form disulfide bridges at the position that superimposes the TrxA binding site in TreX. Our study therefore suggests that thioredoxin 1 evolved alternative functions by maintaining the interaction with cysteine-free substrates.

Secreted bacterial proteins face physical and chemical constraints as they cross the envelope barrier and encounter diverse environments during the transit. As a result, many secreted proteins are partially or completely unfolded during the secretion process and/or use sophisticated machineries that translocate folded proteins. Precise secretion both optimizes the efficiency and reduces the number of environments that the toxin encounters. Bacteria use contact-dependent secretion systems, such as the type VI secretion system (T6SS), to inject toxic protein effectors directly into target cells[1–3]. Structural data have shown that T6SS substrates are folded and recruited to the secretion apparatus in the secreting cell[4,5]. However, it remains unclear whether they remain folded throughout the transport to the target cell. Little is also known about the target cell factors that are required for the entry and/or activity of these toxins, although it is increasingly appreciated that genetic or epigenetic changes can protect the target cell from T6SS attack[6–11].

Most of the T6SS-secreted toxins are highly potent enzymes that target the bacterial cell envelope, energy resources, nucleic acids or protein synthesis machinery[12,13]. In particular, ADP-ribosyltransferase toxins (ARTs) exhibit a remarkable diversity in terms of molecular activities. ARTs use the abundant cellular cofactor NAD^+ to covalently attach the ADP-ribose moiety (ADPr) to various substrates, ranging from proteins to nucleic acids or small molecules (recently reviewed in ref. 14). ADPr adducts are relatively large modifications and therefore interfere with the proper function of their cellular targets. Immunities that protect against the ADP-ribosylation activity can be small proteins that bind tightly to the toxin and block its active site[15,16] or relaxed specificity ADP-ribosyl-hydrolases that protect against a wide range of ART toxins[17]. T6SS-secreted ARTs targeting the cell division protein FtsZ, the translation elongation factor EF-Tu, the 23S ribosomal RNA, or other structured non-coding RNAs have been recently reported[15–18]. While these enzymes share a common structural fold and ADP-ribosylation activity, their substrate specificities and neutralization mechanisms are different. ART toxic domains are frequently fused to T6SS-dependent polymorphic Rhs proteins, which form a protective cocoon for toxin delivery. Importantly,

[1]Bacterial Genetics and Physiology, Faculté des Sciences, Université Libre de Bruxelles (ULB), Gosselies, Belgium. [2]Laboratory of Molecular Microbiology and Structural Biochemistry, Institut de Biologie et Chimie des Protéines (IBCP), Université de Lyon, Lyon, France. [3]Laboratoire d'Ingénierie des Systèmes Macromoléculaires (LISM), Institut de Microbiologie de la Méditerranée (IMM), Aix-Marseille Université, Marseille, France. [4]WEL Research Institute, Wavre, Belgique. [5]Present address: Unité Biodiversité et Amélioration des Plantes et Forêts, Centre Wallon de Recherches Agronomiques (CRA-W), Bâtiment Emile Marchal, Gembloux, Belgium. ✉e-mail: laurence.van.melderen@ulb.be; dukas.jurenas@ulb.be

the Rhs toxic domains seem to be poorly folded, and their extraction from the inside of the cocoon likely requires protein refolding[19,20].

Rhs-associated ART toxins have recently been characterized in *Pseudomonas*, *Salmonella,* and *Photorhabdus* species[15,16,18]. Enterobacteria of the genera *Xenorhabdus* and *Photorhabdus* engage in mutualistic relationships with nematodes, which collectively infect and kill a wide range of insects[21,22]. During the infection cycle, bacteria are released into the insect's body cavity where they kill and degrade the cadaver allowing the nematode to mature and reproduce. At the end of the cycle, the bacteria reassociate with their nematode host[23–26]. Despite having specific hosts, the *Xenorhabdus* and *Photorhabdus* genera are closely related, and their genomes are particularly enriched in genes coding for various toxins and pathways for biosynthesis of antimicrobial compounds[27–33]. The T6SS is the major antibacterial weapon as *Xenorhabdus* strains encoding several T6SSs have been shown to outcompete less equipped strains in intra-bacterial competition[34,35]. The *X. bovienii* (Xb) SS-2004 genome (taxid: 406818)[27] encodes two T6SS gene clusters and three associated Rhs toxins.

In this work, we show that the *X. bovienii* Rhs toxin TreX is an ADP-ribosyltransferase that modifies the cell division protein FtsZ. Strikingly, we found that the enzymatic activity of TreX is strictly dependent on the conserved thioredoxin 1 (TrxA), a small oxidoreductase protein whose primary function in *E. coli* is to reduce disulfide bonds of proteins in the cytoplasm. While many ART toxins rely on disulfide bonds for the cell entry and activation[36–39], TreX does not contain any cysteine. Nevertheless, our functional and structural studies reveal that TrxA binding is essential for the ADP-ribosylation activity and the toxicity of TreX, although it does not prevent its neutralization by the cognate TriX immunity protein. Comparisons of sequences and structural models suggest that a family cysteine-free TreX-like toxins bind thioredoxins in a conserved manner. Furthermore, these toxins share an evolutionary origin with the Scabin toxin that is produced by the plant pathogen *Streptomyces scabies*[40]. Strikingly, a disulfide bridge at the thioredoxin interaction site is conserved in Scabin-like toxins, further suggesting evolutionary links between thioredoxin chaperone clients and redox substrates.

Results

X. bovienii encodes three T6SS-associated Rhs toxins

Rhs elements, long-time known as genomic rearrangement hotspots, were later shown to encode polymorphic toxins that form a molecular cocoon enclosing a hypervariable C-terminus[19,20,41]. Such C-termini constitute toxic domains that are delivered to target cells upon intercellular competition[42,43]. We have screened the *X. bovienii* SS-2004 genome for Rhs homologs and found three full-length Rhs genes, each coding for a different C-terminal toxic domain (Fig. 1a). One of the Rhs toxins (XBJ1_0281) is encoded in the T6SS-1 gene cluster downstream of the genes coding for the spike protein VgrG and the cognate EagR chaperone family, while the two others (XBJ1_1298 and XBJ1_1305) are encoded in an accessory genomic island downstream of the genes coding for VgrG and cognate DUF2169 family T6SS-adaptor proteins (Fig. 1a). The Rhs C-terminal domains are delimited by two DPxGL motifs separated by 17 amino acids that constitute the autoproteolytic motif responsible for the release of the toxic domain into target cells[19,42]. The Rhs encoded in the T6SS-1 gene cluster (XBJ1_0281) comprises a C-terminus with predicted HNH nuclease domain, while the accessory Rhs proteins (XBJ1_1298 and XBJ1_1305) comprise predicted NAD^+ hydrolase and ADP-ribosyltransferase domains, respectively. Overproduction of these domains in the *E. coli* cytoplasm confirmed that the three *X. bovienii* Rhs proteins encode active C-terminal toxins (Fig. 1b).

X. bovienii TreX belongs to the R-S-E clade of ADP-ribosyltransferases

At least four different toxicity mechanisms have been recently reported for T6SS-secreted ARTs[15–18]. Most of the ART enzymes can be categorized into two major evolutionary clades—H-Y-[QED] and R-[ST]-E, based on their active site amino acid residues[44]. Protein sequence analysis highlighted the conservation of the R-S-E catalytic triad in the toxic domain of XBJ1_1305, which was therefore renamed TreX for T6SS ADP-ribosylating effector from *X. bovienii* (Fig. 1c). This toxin belongs to the same evolutionary clade as the previously described Tre1 toxin of *S. proteamaculans* which is delivered by the T6SS[17,44]. Similarly to Tre1, the R-S-E catalytic triad of TreX further forms a characteristic ExE motif typical of arginine-modifying ADP-ribosylating toxins (Fig. 1c). This motif, located in the so-called ADP-ribosyl turn-turn (ARTT) loop, is critical for protein substrate recognition and catalysis[45,46]. The first glutamate is needed for the transferase reaction, while the second is essential for both NAD^+ hydrolysis and ADPr transfer[47,48]. In TreX, the glutamate dyad corresponds to E100 and E102 residues of the toxic ART domain or E1479 and E1481 of the full-length Rhs protein. Supporting these predictions, alanine substitutions of each of these two glutamate residues abolished TreX toxicity (Fig. 1d).

The TriX immunity protein neutralizes TreX by occluding its active site

The previously reported *S. proteamaculans* Tre1 toxin is neutralized by the cognate bi-functional immunity protein Tri1, composed of a N-terminal toxin-binding domain that blocks the toxin by inserting into its active site and a C-terminal ADP-ribosylhydrolase domain that enzymatically removes ADPr adducts[17]. The XBJ1_1304 ORF (hereby renamed *triX*) was identified downstream of *treX* but did not present any conserved sequence signatures or domains. Co-production of TriX prevented TreX-dependent growth inhibition (Fig. 1d), demonstrating that TriX acts as an immunity protein.

To better understand the structural and mechanistical differences between the Tre1-Tri1 and TreX-TriX toxin-immunity pairs, the TreX-TriX complex was purified and crystallized. The 1.3 Å-resolution structure revealed that the TreX toxin displays conserved features of the ART fold (Fig. 1e): a central twisted β-sheet folded in the order of 4-5-2/1-3-6[44]. While TreX structure followed the overall order of this fold, it lacked the β4 strand that was replaced by a buckled loop with α-helical features docking against another α-helix connecting the β1-β2 strands. Compared to the canonical ART fold, TreX presented a C-terminal extension that folds into a β-strand (β7) thereby expanding its central β-sheet (Supplementary Fig. 1). The putative catalytic triad and the ARTT loop were located at the end of the β1-strand (R15), at the center of the β2-strand (S54) and at the beginning of the β5-strand (E100, E102) (Supplementary Fig. S1). All these residues are oriented towards the cleft of the twisted β-sheet typically accommodating the NAD^+ cofactor. Despite sharing identical active site composition, the Tre1 and TreX toxins share limited structural similarity. Specifically, the Tre1 toxin has additional N-terminal elements, and its C-terminal β-strand inserts between β3 and β4-strands that extends the central β-sheet (Supplementary Fig. 1). As compared to other structurally characterized ART toxins, the closest structural homologs of TreX are the DNA-targeting toxins Scabin from *Streptomyces scabies*[49] and ScARP from *Streptomyces coelicolor*[50] as well as the N-terminal (D1) domain of *Mycoplasma pneumoniae* CARDS toxin, targeting the inflammasome component NLRP3[51,52] (Supplementary Fig. 1).

The structure also revealed that unlike Tri1, the TriX immunity protein does not possess an ADP-ribosyl hydrolase fold (Fig. 2e, Supplementary Fig. 2). Instead, it adopts a compact wedge shape formed by a N-terminal twisted β-sheet, followed by a mixed, mostly α-helical, fold which complements the surface of the cognate TreX toxin. Despite similarities between their cognate toxins, the immunity proteins TriX and Tri1 are unrelated (Fig. 1e, Supplementary Fig. 2). As mentioned above, Tri1 is a bimodular immunity protein and was previously shown to be capable of reversing ART-catalyzed modification by non-cognate toxins[17]. Indeed, co-expression of Tri1

https://doi.org/10.1038/s41467-024-54892-w

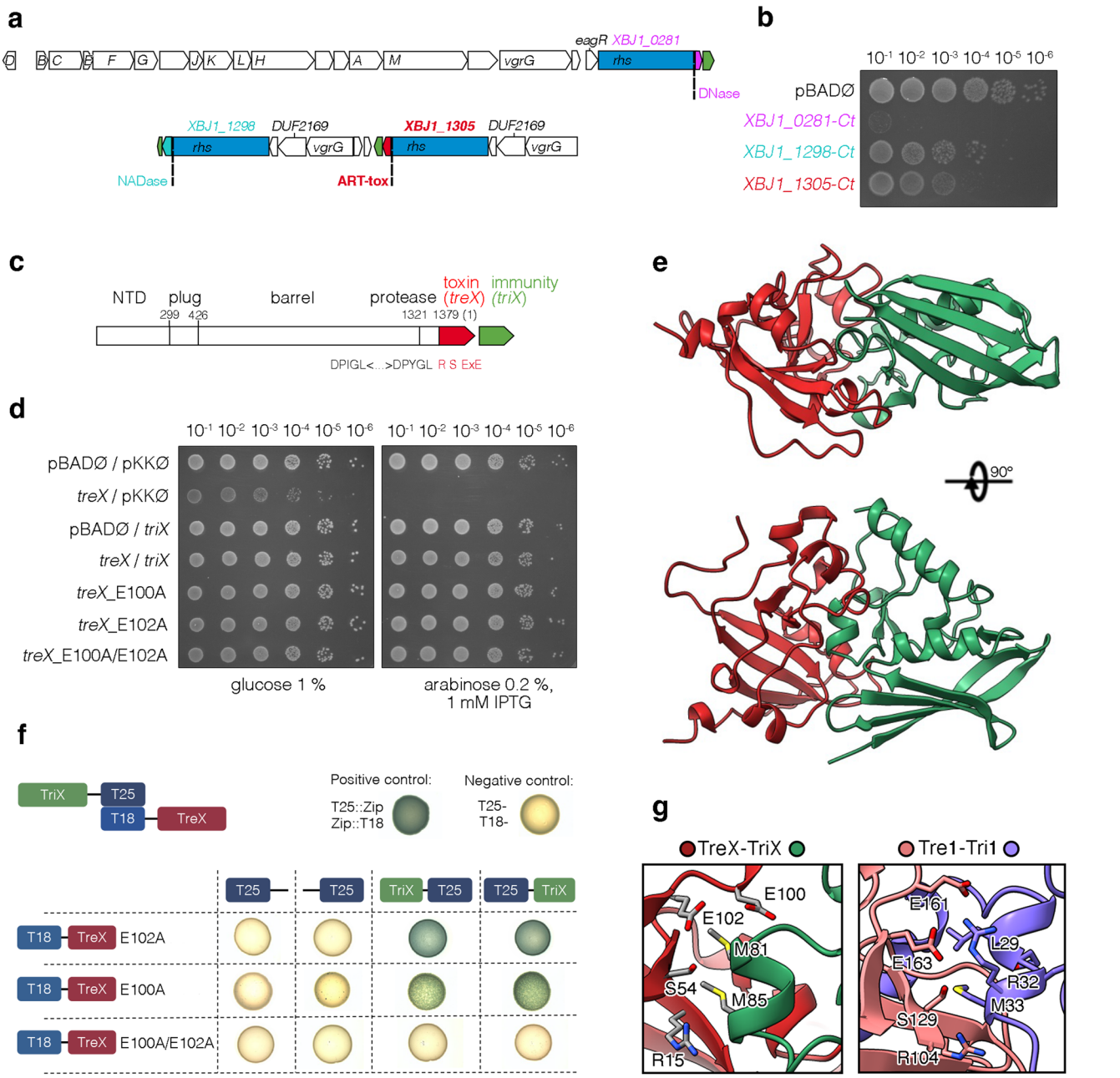

Fig. 1 | The *Xenorhadbus bovienii* TreX putative ADP-ribosyltransferase toxin is neutralized by the TriX immunity protein. a Schematic representation of *X. bovienii* SS-2004 T6SS gene clusters. Rhs are shown in blue, their C-terminal toxic domains (Ct) in purple, cyan, red, and genes encoding their putative cognate immunity proteins are shown in green. The putative activities of the Rhs C-terminal domains are indicated. Genes encoding other T6SS components are indicated as follows: A for TssA, B for TssB, etc. **b** Rhs C-terminal domains inhibit growth of *E. coli* when heterologously expressed from pBAD33 vector. Serial dilutions of overnight bacterial cultures carrying vectors coding for different Rhs C-terminal toxins were spotted on LB plates supplemented with 0.2% L-arabinose. **c** Schematic representation of XBJ1_1305 *rhs* gene emphasizing the different predicted protein domains—N-terminal domain (NTD) related to protein recruitment to the T6SS, N-terminal plug domain, Rhs fold forming β-roll barrel, aspartyl-transferase (protease) and ADP-ribosyltransferase (ART) toxin domain (red). Pre-toxin sequence carrying DPxGL motifs required for auto-proteolysis leading to toxin release and conserved R-S-ExE residues characteristic to the active site of RSE-clade enzymes are indicated. **d** Cultures of *E. coli* MC4100 wild-type cells producing wild-type TreX or its E101A, E103A or E101A/E103A mutants from the pBAD33 vector, and TriX (XBJ1_1304) from the pKK223-3 vector were serially diluted and spotted on LB plates supplemented with 0.2% L-arabinose and 1 mM IPTG. **e** Crystal structure of TreX (corresponding to XBJ1_1305 C-terminal domain, residues 1380–1518; red) in complex with its immunity protein TriX (green). **f** Bacterial two hybrid (BACTH) assay. BTH101 reporter cells producing combinations of the indicated T18 and T25 fusion proteins were spotted on LB agar plates supplemented with IPTG and X-Gal. The blue color of the colonies reports an interaction between the two partners. **g** Zoom-in of the TreX (left) and Tre1 (right) active sites highlighting the position of the inhibiting α-helices of the corresponding immunities (TriX residues 80–85, green; Tri1 residues 27–33, blue, PDB code: 6DRH). The sidechains of the R-S-ExE active site residues of the toxins and the residues of the immunity proteins are indicated.

could partially restore TreX-induced growth inhibition (Supplementary Fig. 2). In addition to its ADPr-hydrolase activity, Tri1 also inhibits Tre1 via physical interactions[17]. The Tri1 and TriX α-helices (residues 27–33 and 80–86 respectively) responsible for this inhibition insert into the active site in close contact with the R-S-ExE catalytic site residues, although the amino acid sequences of these helices are different (Fig. 1g, Supplementary Fig. 2). Strikingly, mutations of the TreX active site residues E100A and E102A

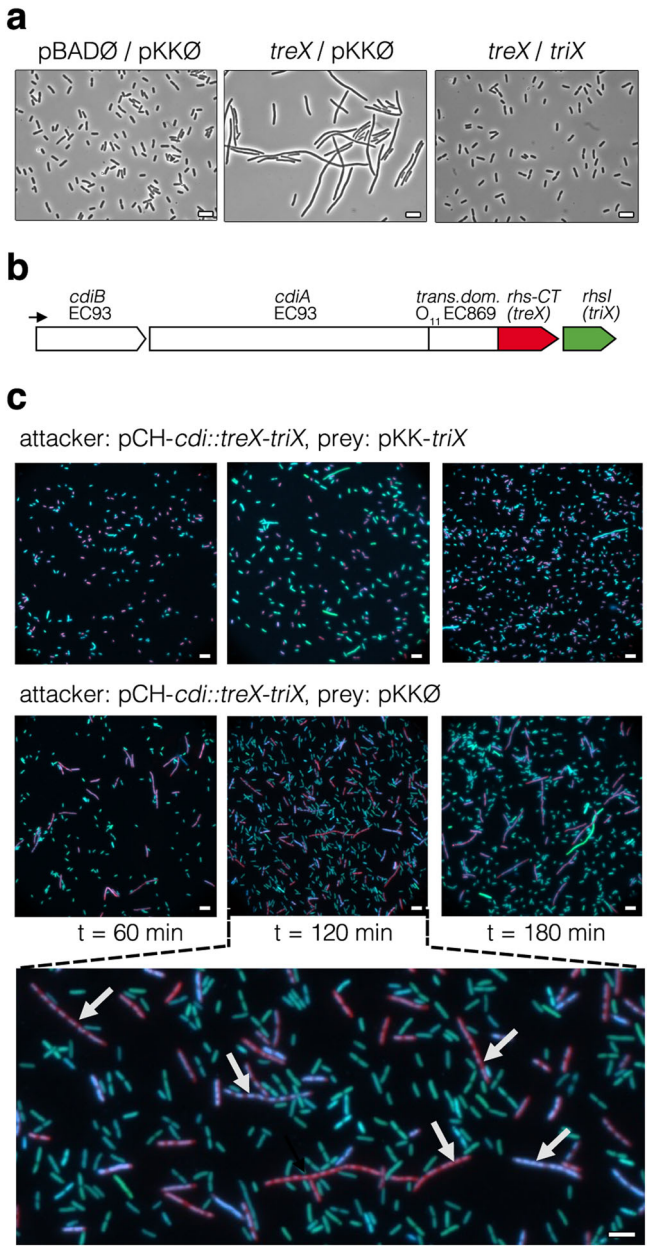

Fig. 2 | TreX induces cell filamentation. a Heterologous expression of the TreX toxin induces *E. coli* filamentation. Microscopy recordings of *E. coli* cells 60 min after induction of the expression of *treX* and *triX*, as indicated. **b** Schematic representation of the chimeric two component *cdiA-cdiB* contact dependent growth inhibition system. The *treX* sequence (residues 1380–1518 of *X. boviennii* XBJ1_1305, red) is branched to the C-terminus of the EC93 *cdiA*, downstream the translocation domain. The gene coding for immunity protein TriX (green) is placed downstream to protect the secreting cells. **c** The chimeric Cdi::TreX-TriX system is functional in bacterial competition against *E. coli*. Target MG1655 Nal^R pT5::mCherry cells expressing the *triX* gene from the pKK223-3-*TriX* vector are protected (top panel), while those carrying the empty pKK223-3 (middle panel) are killed. Attacker cells expressing the TreX toxin from the pCH vector are shown in cyan, while target cells are shown in cherry, merged with blue for DAPI straining of the nucleoid. Arrows in the zoom-in panel below point to filamenting target cells, resulting from arrested cell division. Scale bars, 5 µm.

abolished the toxin-immunity interaction as revealed by bacterial two-hybrid assay (Fig. 1f), demonstrating the specificity and importance of the interactions at the active site of the toxin for neutralization by the TriX immunity protein (Fig. 1f, g).

TreX causes cell filamentation independently of the induction of the SOS response

To further explore the molecular mechanism by which TreX inhibits cell growth, we first checked for the phenotypes induced by the production of TreX. Microscopy observations showed that the overproduction of TreX in *E. coli* resulted in massive cell filamentation, which is indicative of inhibition of cell division (Fig. 2a). Filamentation can potentially result from the induction of the SOS response upon DNA damage, via the expression of the SOS-regulated cell division inhibitor SulA. Such phenotype could be expected if the target of TreX was DNA, as in the case of Scabin-like toxins[40] that we found to be the closest structural homologs of TreX (Supplementary Fig. 1). However, DAPI staining and time-lapse microscopy recordings revealed that DNA was replicated and segregated in TreX-induced filaments (Supplementary Fig. 3). Using a SOS-reporter (P*sulA*-GFP), we further confirmed that the SOS response was not activated upon overproduction of TreX as compared to the effect of an ofloxacin treatment used as a control (Supplementary Fig. 3). Finally, *lexA3* mutant cells that are unable to induce the SOS response and therefore to filament upon DNA damage, still displayed the filamentation phenotype upon overproduction of TreX (Supplementary Fig. 3). Alternatively, filamentation could be caused by a direct inhibition of the cell division machinery, as it was shown for the Tre1 toxin which ADP-ribosylates the cell division protein FtsZ thereby corrupting its polymerization[17]. We therefore tested whether TreX ADP-ribosylates FtsZ in vitro. Our attempts to detect ADP-ribosylation of purified FtsZ in vitro by addition of the TreX toxin and biotinylated NAD^+ were not successful. However, incubation of TreX with *E. coli* crude protein extract revealed multiple modified proteins, among which a band at the size of FtsZ, indicating that the activity of TreX might rely on an unknown factor present under these conditions but absent in the in vitro assay with purified proteins (Supplementary Fig. 4).

TrxA mutants are resistant to TreX

To identify potential cellular cofactors necessary for TreX activity, we thought to isolate TreX resistant mutants in *E. coli*. We have established a double selection system based on the endogenous production of TreX as a first step and a competition with an attacker strain secreting the TreX toxin as the second step, to reduce the number of false positives (e.g., mutants in the toxin gene or defective for toxin expression). Since *X. bovienii* SS-2004 strain encodes multiple Rhs and genetic manipulations of *Xenorhabdus* proved to be difficult, we developed a simple system that could be used for the second selection step. Since the T6SS machinery is sophisticated, the effector loading mechanisms not fully understood and clusters are very large, we exploited another contact dependent growth inhibition system—CDI, which is composed of two proteins CdiA and CdiB[53]. CdiA is a long molecular stick that contains a C-terminal toxic domain delimited by a conserved VENN motif[53,54]. CdiB is the outer membrane β-barrel transporter that delivers the CdiA protein at the cell surface. Toxin-encoding genes from CDI systems are followed by cognate immunity-encoding genes in *cdi* clusters which protects cells against self-intoxication[53]. Rhs and CDI therefore possess common features in architecture and organization. We have grafted the *treX-triX* toxin-immunity gene pair on the well-characterized *E. coli* EC93 CDI system under the control of its native promoter[55]. Briefly, the chimeric CDI system contains 3 distinct modules encoded on a plasmid: (i) CdiB, (ii) the $CdiA_{EC93}$ structural protein fused to the translocation domain of *E. coli* EC869 ($cdiA_{O11}^{EC869}$) known to support the delivery of different CDI toxins into *E. coli* cells, which is further fused to TreX, and (iii) the downstream encoded TriX immunity (Fig. 2b). To test the functionality of the chimeric CDI, competition experiments were performed between a MG1655 strain containing the chimera and constitutively expressing GFP and a MG1655 strain expressing mCherry. The phenotype induced by the chimeric CDI::TreX system (CDI^+) in target cells

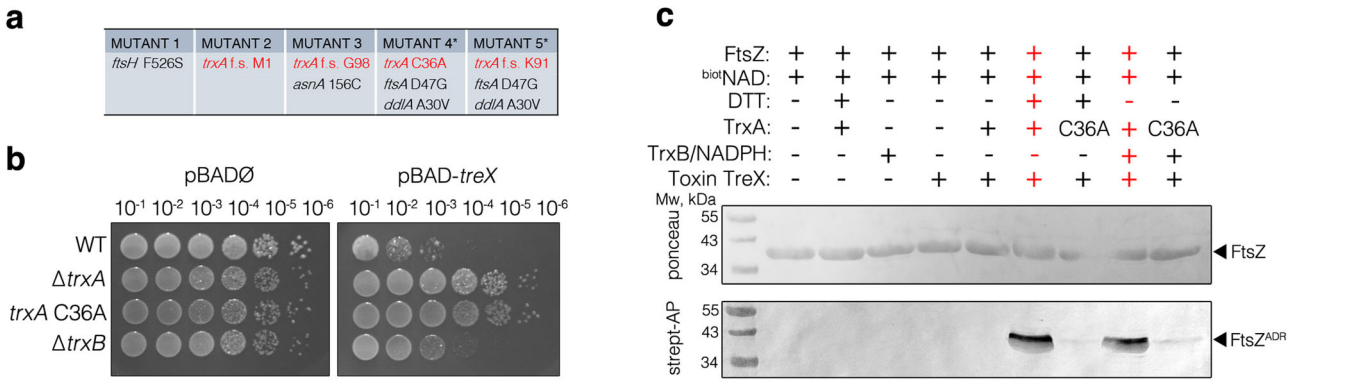

Fig. 3 | The reduced form of TrxA is required for TreX activity. a Mutations of five independent evolved strains resistant to the chimeric CDI::TreX-TriX system selected in bacterial competition. Genes and corresponding mutations are indicated (f.s., frameshift after the residue indicated). Asterisks indicate an incomplete list of mutations identified (see Supplementary Table 4 for the complete list of mutations). **b** *E. coli* MC4100 wild-type (WT), *trxA*, *trxA* C36A, and *trxB* mutant strains expressing, or not, *treX* from the pBAD33 vector, were serially diluted and spotted on LB plates supplemented with 0.2% L-arabinose. **c** In vitro ADP-ribosylation of FtsZ by the TreX toxin in various conditions. Purified FtsZ was incubated with the TreX toxin, biotinyl-NAD^+, wild-type or C36A mutant TrxA, reducing agent DTT or TrxB and NADPH, as indicated, for 15 min at 37 °C. Reactions were then subjected to SDS-PAGE, transfer onto nitrocellulose, and stained with Ponceau Red (top panel). Biotinyl-ADP-ribosylation was detected using streptavidin-alkaline phosphate conjugate (lower panel). Molecular weight markers (in kDa) are indicated on the left.

(CDI^-) was similar to that observed when TreX was endogenously produced (Fig. 2c). CDI^- cells expressing *triX* were rescued and could divide normally, confirming the functionality of the chimera (Fig. 2c).

We then proceeded to the double selection combining endogenous expression of *treX* and attack by the CDI::TreX chimera to isolate mutants resistant to TreX. The genomes of 5 resistant clones were sequenced and compared to the wild-type sequence to map the mutations. Surprisingly, 4 out of 5 mutants carried mutations in the *trxA* gene encoding the TrxA, an oxidoreductase that maintains cysteine residues reduced in cytoplasmic proteins (Fig. 3a, Supplementary Table 1). The mutations in *trxA* were different in the 4 mutants sequenced, highlighting the importance of TrxA in the mechanism of TreX toxicity. Interestingly, one of the mutations was the Cys36-to-Ala substitution. The Cys36 residue is part of the CxxC active site motif common to thiol-disulfide oxidoreductases[56]. Two out of the 4 mutants also carried mutation in the *ftsA* (D74G) gene, an essential member of the divisome. The only mutant that did not have an altered *trxA* gene was found to possess a mutation in the *ftsH* (F526S) gene coding for the essential membrane-anchored metalloprotease involved in protein quality control[57]. This mutation is located in a flexible loop in the C-terminal proteolytic domain and is not visible in the structural studies[58]. Overall, the most common mutated gene was *trxA* (Fig. 3a). The TreX resistance phenotype was confirmed in a Δ*trxA* and in a catalytically inactive $trxA_{C36A}$ background (Fig. 3b). Isolation of the $trxA_{C36A}$ mutation points toward the implication of the redox activity of TrxA, although neither the TreX toxin nor the FtsZ suspected target contain cysteine residues. In *E. coli*, the reduced state of TrxA is maintained by TrxB which uses the reducing potential of NADPH[59]. We therefore tested the activity of TreX in a Δ*trxB* mutant. While deletion of *trxA* provided complete protection from TreX toxicity, a *trxB* deletion yielded an intermediate result, indicating that reduction of TrxA is important (Fig. 3b).

TreX ADP-ribosylation activity relies on the reduced form of TrxA

Since TreX was at least partially inactive in the *trxA* and *trxB* mutants, we thus tested whether addition of purified TrxA in an in vitro reaction together with TreX and NAD^+ would lead to the ADP-ribosylation of FtsZ (Fig. 3c). We have purified TrxA and its cysteine mutants (C33A, C36A and the double mutant) under non-reducing conditions. Cysteine derivatization using the thiol specific reagent 4-acetamido-4′-maleimidylstilbene-2,2′-disulfonic acid (AMS) revealed that purified TrxA was oxidized and could be reduced in presence of DTT (Supplementary Fig. 5). While the TreX toxin was inactive alone, the addition of TrxA to the reaction promoted ADP-ribosylation of FtsZ, however only under reducing conditions (with DTT) (Fig. 3c). Mass spectrometry analyses confirmed mono ADP-ribosylation of arginine residues R174, R338, and R379. Residue R174 has also been shown to be ADP-ribosylated by Tre1 and its modification impairs FtsZ polymerization and abolishes septum formation[17]. In agreement with our in vivo data showing partial loss of TreX activity in the Δ*trxB* mutant, we found that in vitro, ADP-ribosylation of FtsZ by TreX was also occurring under conditions in which TrxB reduces TrxA, in the presence of NADPH (Fig. 3c). In agreement with these findings and with the loss of TreX toxicity in the $trxA_{C36A}$ mutant, the $TrxA_{C36A}$ mutated enzyme did not support the in vitro activity of TreX even under reducing conditions (Fig. 3c). We, therefore, concluded that the ADP-ribosylation reaction of TreX strictly depends on the presence of the reduced form of TrxA.

TreX forms a stable complex with the reduced form of TrxA

Even though only the reduced form of TrxA was able to activate TreX, it is unlikely that a TrxA catalyzes a classical redox reaction since neither TreX nor its substrate contain cysteine residues. We therefore hypothesized that reduced TrxA could form a stable complex with TreX responsible for the activation of the toxin. To test this, the inactive TreX toxin (E100A, E102A) fused to a StrepII affinity tag and a His-tagged version of TrxA were co-produced and subjected to co-purification analyses. Both partners could be pulled down by the other—TrxA by the toxin on Strep-tag affinity column and the toxin by TrxA on metal affinity column, showing that they form a stable complex (Fig. 4a). Importantly, production of the TreX toxin alone resulted in a mostly insoluble protein (undetectable in the supernatant fraction), while its soluble fraction pulled down the GroEL chaperone as revealed by mass spectrometry (Fig. 4a). The double affinity purification (Strep-tag followed by metal affinity column) resulted in stoichiometrically equal amounts of TreX and TrxA without any GroEL, suggesting that TrxA assists proper folding and solubility of the TreX toxin (Fig. 4a). Gel filtration analyses supported the existence of a stable 1:1 TreX:TrxA complex of ~30 kDa, with a molecular mass similar to that of the toxin-immunity complex (theoretical masses of 28 kDa and 32 kDa, respectively) (Fig. 4b).

Distinct interaction sites of immunity and TrxA on TreX allow a ménage-à-trois with TreX

As shown in Fig. 1e, the immunity protein TriX occludes the active site of the TreX toxin. To determine whether TrxA binds TreX at the same site, we tested whether TriX could displace TrxA from the TriX-TreX

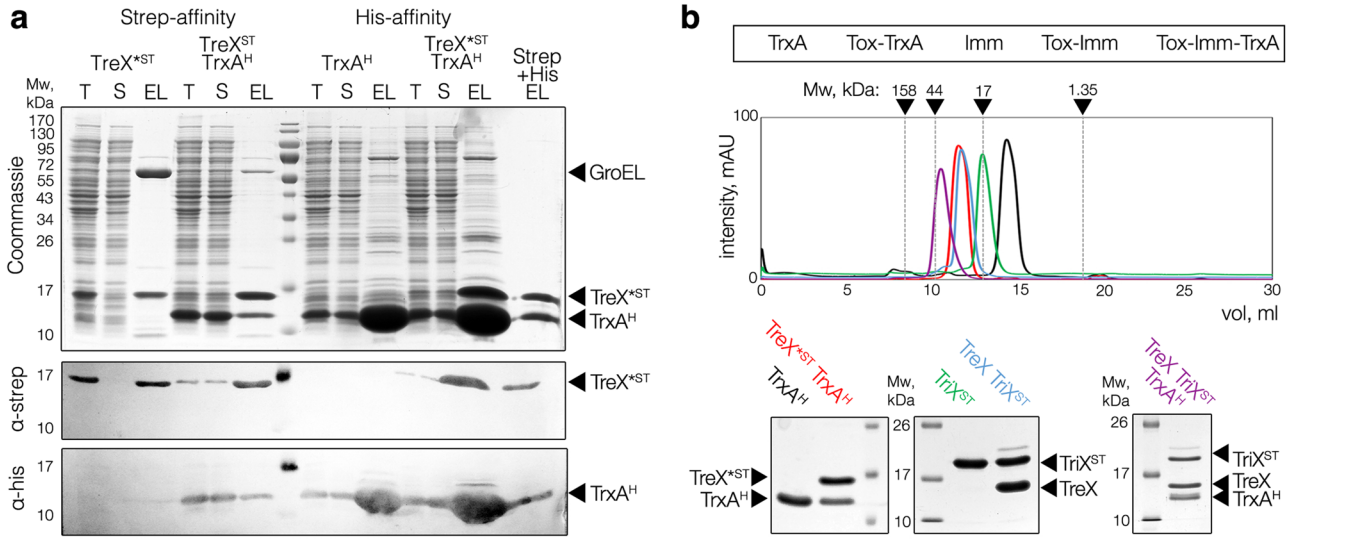

Fig. 4 | The TreX toxin interacts with TrxA. a Pulldown assays. Soluble extracts of cells producing the indicated proteins (TreX^{*ST}, TreX inactive toxin (E102A mutant) fused to a Strep tag; TrxA^{H} (His-tagged *E. coli* TrxA) were subjected to Strep, His, or consecutive Strep and His (Strep + His) affinity purifications. Total (T), soluble (S) and elutions (EL) were separated by SDS-PAGE and stained with Coomassie blue (top panel) or transferred onto nitrocellulose membrane and immunodetected with anti-Strep (middle panel) and anti-His (lower panel) antibodies. The 55-kDa band visible by Coomassie staining was identified as GroEL by mass spectrometry. Molecular weight markers (in kDa) are indicated on the left. **b** Size-exclusion chromatography analysis of purified thioredoxin TrxA (black line), immunity protein TriX (green line), and TreX*-TriX (blue line), TreX*-TrxA (red line) and TreX*-TriX-TxrA (purple line) complexes. Elution volumes of known molecular weight protein standards are indicated. Peak fractions were subjected to SDS-PAGE and Coomassie blue staining (bottom panel) confirmed the presence of the expected proteins.

complex. Such a competition was, however, not observed, as the ternary TriX-TreX-TrxA complex could be readily purified and was stable and homogeneous in solution as analyzed by gel filtration (Fig. 4b), suggesting that TriX and TrxA bind to different sites on TreX. Indeed, the 2.1 Å-resolution crystal structure of the ternary TriX-TreX-TrxA complex showed that TrxA binds distantly from the active site of the toxin and does not make any contact with the TriX immunity, and furthermore that the TrxA and TriX binding sites do not overlap (Fig. 5a). The TreX C-terminal tail extending after the conserved twisted β-sheet provides the main toxin interaction site with TrxA (Fig. 5a, b). This interaction is ensured by the hydrophobic sidechains of the L132 and Y137 C-terminal residues. Most importantly, the T130 residue of TreX interact with the conserved C33 and the neighboring W32 residue of TrxA (Fig. 5b). The contact interface between TreX and TrxA observed in the crystal was further confirmed, as substitutions of TrxA residues engaged in the interaction (W32A, C33A, I61D, D62A, I76D) abolished or strongly reduced binding of the toxin (Fig. 5c). Previous studies of *Salmonella* thioredoxin have also found that residues such as I76 are involved in oxidoreductase activity-independent binding of response regulators of two-component signaling systems[60,61]. In line with our in vivo data, the C36A mutation in TrxA, although not directly involved in the interaction, also abolished binding to TreX. Finally, deletion of the C-terminal extension of the TreX toxin (TreX$_{\Delta CT}$) or substitutions of residues at the interface (T130A, L132A) abolished the interaction with TrxA (Fig. 5c, Supplementary Fig. 6). Altogether, these data indicate that the substrate binding pocket of the reduced form of TrxA recognizes the C-terminal extension of the TreX toxin (Fig. 5b, c). In line with the interaction data, we have found that these TrxA variants did not support the ADP-ribosyltransferase activity of the TreX toxin in vitro (Supplementary Fig. 7).

Importantly, the residues involved in the interactions of the TreX toxin with TrxA are located in the C-terminal extension, far from the ADP-ribosyltransferase active site. This suggests that the TriX immunity protein could neutralize the toxin by binding to its active site, independently of the binding of TrxA. Indeed, we have confirmed that the order of the ménage-à-trois complex formation is not important. The TriX immunity protein can neutralize the TreX toxin or the pre-formed toxin-TrxA complex and vice versa—addition of TrxA does not overcome the neutralization (Fig. 5d). In line with the findings that TriX immunity protein does not possess ADP-ribosyl hydrolase fold (Supplementary Fig. 2), we have found that the addition of the TriX immunity protein after ADP-ribosylation reaction did not remove the covalent ADPr-adducts from the target protein FtsZ (Fig. 5d). On the contrary, purified *S. proteamaculans* ADP-ribosyl hydrolase Tri1 could partially reverse the ADP-ribosylation of FtsZ (Supplementary Fig. 8), which explains its capacity to partially restore growth inhibition mediated by *treX* expression (Supplementary Fig. 2).

The *X. bovienii* TrxA protein shares 62% amino acid sequence identity with its *E. coli* homolog and possesses identical amino acid residues at the interaction surface, except of position 61 where *X. bovienii* thioredoxin carries a valine instead of an isoleucine in *E. coli* TrxA (Supplementary Fig. 9). Nevertheless purified *X. bovienii* TrxA had identical effects on the enzymatic activity of TreX, and immunization could also be achieved using TriX (Supplementary Fig. 9). Furthermore, the 1.9 Å-resolution crystal structure of the TriX-TreX-TrxA$_{Xb}$ ternary complex revealed conserved interactions between the TreX toxin and thioredoxins from different species (Supplementary Fig. 9).

TrxA is a chaperone for TreX

As shown above, the TreX toxin interacts with the conserved substrate binding site of TrxA. This complex is required for both the solubility and the activity of TreX, suggesting that TrxA plays the role of a molecular chaperone stabilizing TreX and supporting its activity. To rule out the possibility of a TrxA redox reaction during TreX-mediated catalysis, we tested whether the TreX-TrxA complex can support multiple rounds of ADP-ribosylation reaction. The wild-type TreX toxin was separated from the purified TreX-TriX complex and refolded in the presence of an excess of TrxA under reducing conditions. The TreX-TrxA complex was then separated from the excess of TrxA and DTT by gel filtration. Freshly prepared TreX-TrxA complex was then added in increasing amounts to reactions containing a fixed concentration of

https://doi.org/10.1038/s41467-024-54892-w

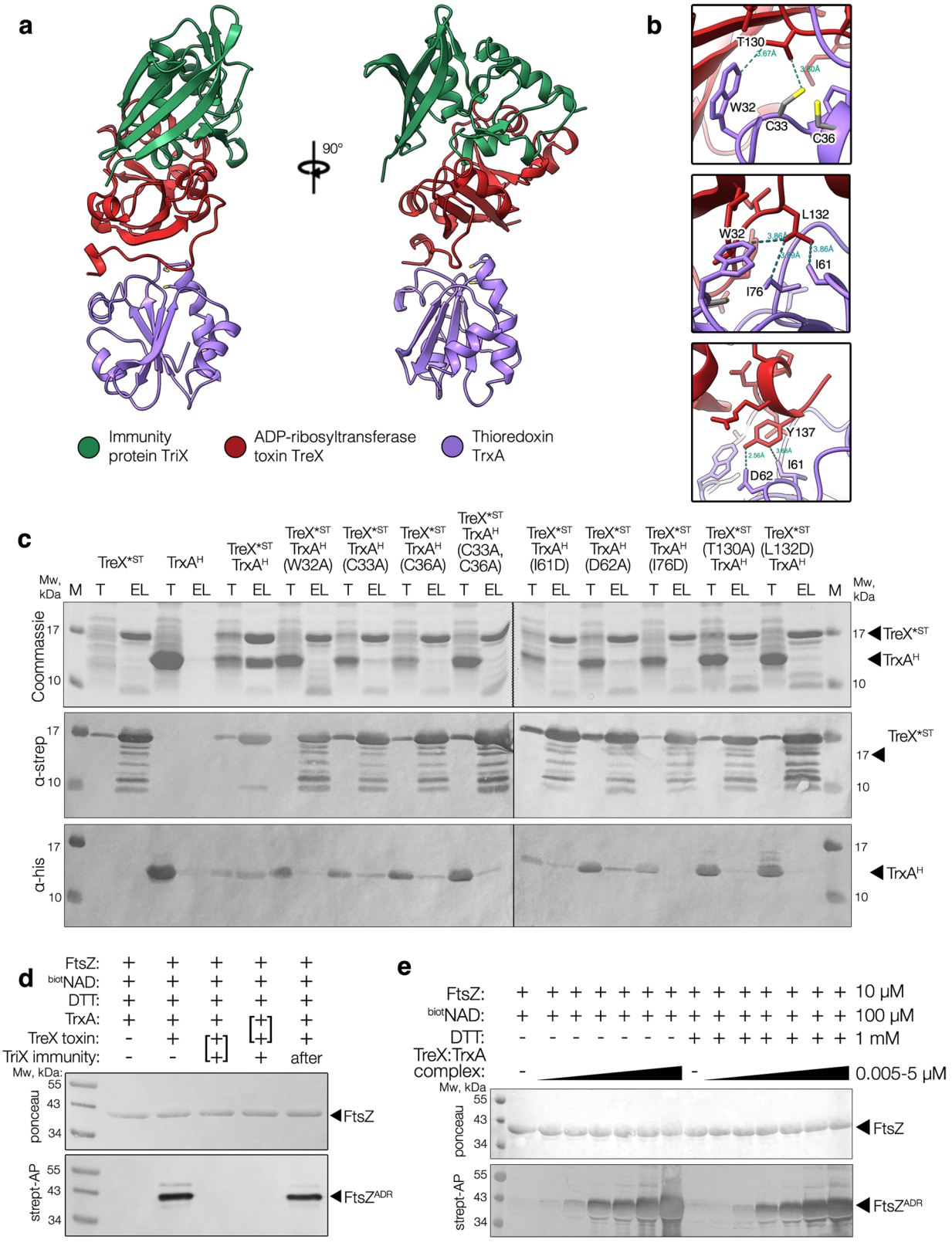

FtsZ, the target of TreX. If a redox reaction was necessary for the ADP-ribosylation reaction, the amount of modified FtsZ should be strictly equimolar to the amount of TreX-TrxA complex, meaning that one molecule of reduced complex would only modify one molecule of target, and the addition of DTT to the reactions would increase the ADP-ribosylation of FtsZ because of TrxA recycling. Enzymatic assays, however, indicated that pre-formed TreX-TrxA complex worked at its maximum capacity, since the addition of DTT did not increase the reaction rate at any concentration of the TreX-TrxA complex tested (Fig. 5e). These results further support the role of TrxA as a chaperone and argue against the involvement of redox reactions in the enzymatic activity of the TreX toxin.

Fig. 5 | Structural characterization of the TreX-TriX-TrxA tripartite complex. **a** Crystal structure of TreX toxin (red) in complex with its immunity protein TriX (green) and *E. coli* thioredoxin TrxA (purple). **b** Zoom-in of the interaction site between the C-terminal residues of the TreX toxin and TrxA, highlighting a series of hydrophobic interactions and hydrogen bonds: TreX T130 forms hydrogen bond with TrxA catalytic C33 (left panel), TreX L132 forms a series of hydrophobic interactions with TrxA W32, and I61 and I76 side chains (middle panel), TreX Y137 sidechain forms hydrogen bond and hydrophobic interactions with TrxA D62 and I61, respectively (right panel). **c** Pulldown assays. Soluble extracts of cells producing the TreX^{*ST} and TrxA^{H} or their mutated versions were subjected to Strep affinity purification. Total extracts (T) and elutions (EL) were separated by SDS-PAGE and stained with Coomassie blue (top panel) or transferred onto nitrocellulose membrane and immunodetected with anti-Strep (middle panel) and anti-His (lower panel) antibodies. Molecular weight markers (in kDa) are indicated on the left. **d** In vitro neutralization of the toxin before or after interaction with TrxA. TreX was pre-incubated with the TriX immunity or with TrxA before adding the other components (FtsZ, biotinyl-NAD$^+$, DTT) when indicated with brackets. The immunity protein was also added after the incubation of the toxin and TrxA under reducing conditions, and the reaction was continued for 30 min (right lane). **e** In vitro ADP-ribosylation of FtsZ with increasing amounts of TreX-TrxA complex reconstituted under denaturing conditions and purified in buffer without DTT. Reactions containing constant amount of FtsZ and biotinyl-NAD$^+$ were mixed with or without the reducing agent DTT for 30 min at 37 °C. The ADP-ribosylation of FtsZ was detected by western-blot using streptavidin-alkaline phosphate conjugate.

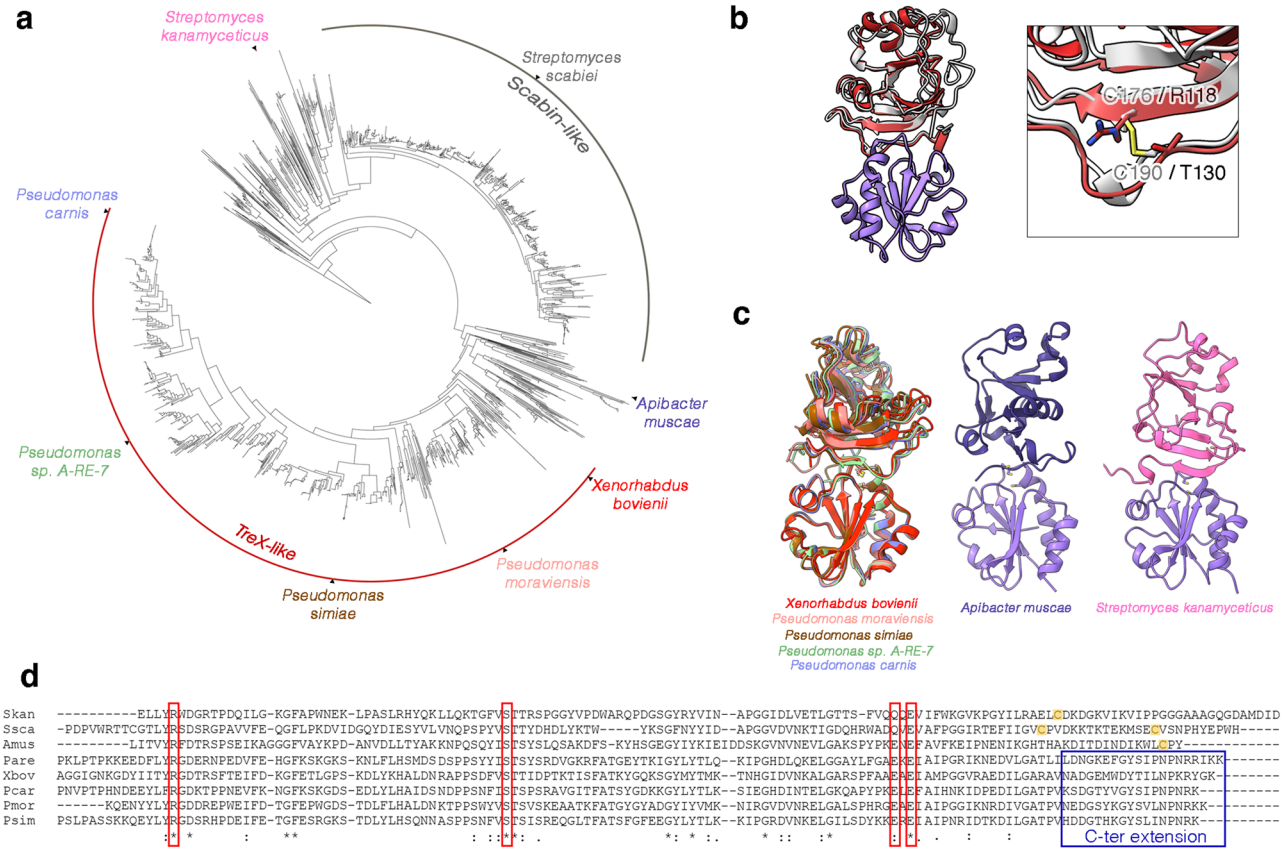
a
Streptomyces kanamyceticus
Streptomyces scabiei
Scabin-like
Pseudomonas carnis
Apibacter muscae
Pseudomonas sp. A-RE-7
Xenorhabdus bovienii
TreX-like
Pseudomonas moraviensis
Pseudomonas simiae
b
C176/R118
C190 / T130
c
Xenorhabdus bovienii
Pseudomonas moraviensis
Pseudomonas simiae
Pseudomonas sp. A-RE-7
Pseudomonas carnis
Apibacter muscae
Streptomyces kanamyceticus
d
Skan ----------ELLYRWDGRTPDQILG-KGFAPWNEK-LPASLRHYQKLLQKTGFVSTTRSPGGYVPDWARQPDGSGYRYVIN--APGGIDLVETLGTTS-FVQCEVIFWKGVKPGYILRAELCDKDGKVIKVIPPGGGAAAGQGDAMDID
Ssca -PDPVWRTTCGTLYRGDSRGPAVVFE-QGFLPKDVIDGQYDIESYVLVNQPSPYVSTTYDHDLYKTW-----YKSGFNYYID--APGGVDVNKTIGDQHRWADCMEVAFPGGIRTEFIIGVCPVDKKTKTEKMSECVSNPHYEPWH-----
Amus --------LITVYRFDTRSPSEIKAGGGFVAYKPD-ANVDLLTYAKKNPQSQYISTSYSLQSAKDFS-KYHSGEGYIYKIEIDDSKGVNVNEVLGAKSPYPKEMEFAVFKEIPNENIKGHTHAKDITDINDIKWLCPY----------
Pare PKLPTPKKEEDFLYRGDERNPEDVFE-HGFKSKGKS-KNLFLHSMDSDSPPSYYISTSYSRDVGKRFATGEYTKIGYLYTLQ--KIPGHDLQKELGGAYLFGAEKEIAIPGRIKNEDVLGATLLILDNGKEFGYSIPNPNRRIKK-------
Xbov AGGIGNKGDYIITYRGDTRSFTEIFD-KGFETLGPS-KDLYKHALDNRAPPSDFVSTTIDPTKTISFATKYGQKSGYMYTMK--TNHGIDVNKALGARSPFAAEMEIAMPGGVRAEDILGARAVNADGEMWDYTILNPKRYGK-------
Pcar PNVPTPHNDEEYLFRGDKTPPNEVFK-NGFKSKGDS-EDLYLHAIDSNDPPSNFISTSPSRAVGITFATSYGDKKGYLYTLK--SIEGHDINTELGKQAPYPKEIEFAIHNKIDPEDILGATPVKSDGTYVGYSIPNPNRK----------
Pmor ------KQENYYLYRGDDREPWEIFD-TGFEPWGDS-TDLFLHALDNKTPPSWYVSTSVSKEAATKFATGYGYADGYIYVMK--NIRGVDVNRELGALSPHRGEMEIAIPGGIKNRDIVGATPVNEDGSYKGYSVLNPNRKK----------
Psim PSLPASSKKQEYLYRGDSRHPDEIFE-TGFESRGKS-TDLYLHSQNNASPPSNFVSTSISREQGLTFATSFGFEEGYLYTLK--KIPGRDVNKELGILSDYKKEPEIAIPNRIDTKDILGATPVHDDGTHKGYSLINPNRK----------
C-ter extension

Fig. 6 | Conserved interactions of TreX-like toxins with thioredoxins. **a** Cladogram of TreX toxin homologs ($n = 2195$). TreX-like ($n = 1027$) and Scabin-like ($n = 707$) clades are suggested based on the absence or the presence of potential disulfide bridge at the C-terminus respectively. **b** Structure of TreX (red) bound to TrxA (purple) is superimposed to the structure of the toxin Scabin (gray, PDB code: 6VV4). Scabin residues involved in disulfide bridge formation (C176 and C190) align with residues R118 and T130 of TreX, as shown in the zoom-in (right panel). **c** AlphaFold predicted models of TreX and Scabin-toxin homologs in complex with their cognate thioredoxins. *X. bovienii* complex (left, colored in red) was solved by X-ray crystallography and aligned to models of homologs from *Pseudomonas* spp. All AlphaFold prediction statistics are provided in Supplementary Fig. 11 and Supplementary Table 5. **d** Amino acid sequence alignments of TreX and Scabin toxin homologs. Active site residues are boxed in red, C-terminal extensions interacting with thioredoxins are boxed in blue, cysteines are highlighted in yellow.

The TreX homolog Scabin possesses disulfide bond at the TrxA binding region

Our structural and biochemical observations indicated that TrxA acts as a chaperone by forming a stable, soluble, and active complex with the TreX toxin. TrxA has been previously shown to bind to the DNA-polymerase of bacteriophage T7 and to act as a processivity factor by significantly increasing its polymerization efficiency[62]. However, it remains unclear how TrxA, which is an oxidoreductase, evolved this function. To better understand the emergence and the conservation of a chaperone role for TrxA in the context of ART toxins, we analyzed sequences of homologs of TreX. Phylogenetic tree of TreX-homologs showed two main clusters that could have emerged from a common ancestor. Proteins similar to the *X. bovienii* TreX toxin are widely distributed in *Pseudomonas* spp. and mostly in architecture with Rhs domains (Fig. 6a, Supplementary Table 5). On the contrary, proteins similar to the Scabin toxin are widely distributed in *Streptomyces* spp. and constitute a different cluster (Fig. 6a). Of note, *S. proteamaculans* Tre1 toxin was not retrieved in our homology search, indicating that it has limited sequence similarity to TreX.

Three-dimensional superimposition of the Scabin toxin with the TreX-TrxA complex revealed that both toxins fit equally into the active site of TrxA (Fig. 6b). Interestingly, C-terminal extensions in Scabin-like toxins contain 2 cysteines (C176 and C190 for Scabin) that form a disulfide bridge and align to residues R118 and T130 of TreX

(Fig. 6b). It is worthy to note that the T130 side chain of TreX is in direct contact with the C33 of the CxxC motif of TrxA (Fig. 5b). Although the activity of Scabin has not been reported to be dependent on TrxA or cysteine redox state, the C176-C190 disulfide bridge has been suggested to be important for Scabin structural stability[40]. However, the formation or reduction of this disulfide bridge in vivo and its potential role in enzymatic activity of Scabin have not been reported. In comparison to Scabin, we speculated that the R118 and T130 residues in TreX might correspond to cysteines that formed a disulfide bridge in a TreX ancestor, providing the stabilizing function. However, the substitutions of T130 and R118 to cysteines did not abolish the dependency for TrxA (Supplementary Fig. 10).

Interaction with thioredoxins is conserved in TreX homologs

We have further analyzed several more distant TreX and Scabin homologs. To this end, we have used AlphaFold[63] to model the structures of these proteins in complex with thioredoxins from their cognate species. Based on our predictions, most of the homologs fall into the TreX-like cluster that lacks cysteines and potentially depends on interaction with TrxA, and into the Scabin-like cluster that contains disulfide bridge at position comparable to R118-T130 residues in TreX (Fig. 6a). Indeed, putative TreX-like toxins from *Pseudomonas* spp. were all predicted to form highly similar complexes with thioredoxins, despite variations in their C-terminal sequences (Fig. 6c, d, Supplementary Fig. 11). Expression of *P. moraviensis* R28 Rhs C-terminal TreX-like toxin domain $TreX_{Pm}$ (locus tag: PMO01_08745) in *E. coli* WT and TrxA mutant strains confirmed that its activity depends on TrxA (Supplementary Fig. 12). Surprisingly, $TreX_{Pm}$ failed to ADP-ribosylate FtsZ in vitro even in presence of reduced TrxA. In contrast, activity of the previously reported Tre1 toxin, which did not appear as a TreX-homolog during our bioinformatic search, did not depend on TrxA (Supplementary Fig. 12). We have speculated that the $TreX_{Pm}$ toxin could have alternative cellular target(s). Indeed, ADP-ribosylation reaction of cellular extracts of *E. coli*, *X. bovienii* and *P. moraviensis* with the three toxins revealed that $TreX_{Pm}$ shows a different ADP-ribosylation pattern, while Tre1 and $TreX_{Xb}$ primarily modified a protein at the size of FtsZ (Supplementary Fig. 12). It is important to note that $TreX_{Xb}$ was inactive in *X. bovienii* extract, while $TreX_{Pm}$ was inactive in *P. moraviensis* extract, which is likely due to the expression of their cognate immunity proteins by these strains. In line with the observations that $TreX_{Pm}$ does not modify FtsZ, its expression in *E. coli* did not cause cell filamentation, and instead resulted in appearance of empty "ghost" cells (Supplementary Fig. 12). Interestingly, the distantly related Scabin-like toxins were reported to ADP-ribosylate DNA[40,49], which suggests that the ART toxins in this family might have evolved many different substrate specificities. While the active site residues are characterized and conserved between different ART toxin homologs (Fig. 6d), what are the determinants of substrate specificity remains to be discovered.

Of note, some TreX and Scabin homologs did not fall into any of the two clades and showed much more variations in terms of their structures, domain-architectures and phylogenetic distribution (Supplementary Table 5). Surprisingly, we have found that some proteins in these clusters carry only the first or the second cysteine residues corresponding to position of disulfide bridge in Scabin (Fig. 6c, d). Nevertheless, AlphaFold models predict conserved modes of interaction with their cognate thioredoxins (Fig. 6c). Overall, our data suggests that the association of TreX-like toxins with thioredoxins is more conserved than their target specificity. More generally, our data demonstrate that TrxA binds its redox substrates in a manner similar to its chaperone clients, such as T7 DNA-polymerase[64], *Salmonella* response regulators[60,61] and TreX-like toxins (Fig. 7a). The phylogenetic relationship of TreX to other toxins that have cysteines, such as Scabin (Fig. 6b, c) further suggests that the TrxA chaperone clients are likely to have evolved from ancestral redox substrates.

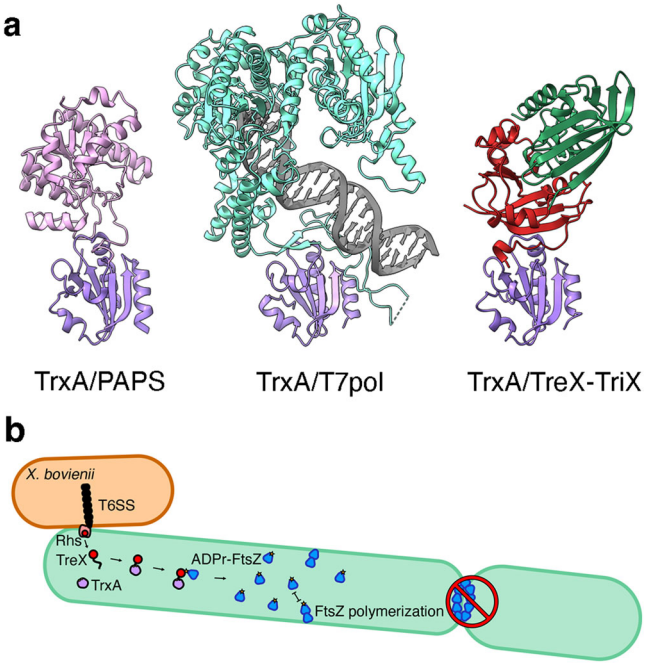

Fig. 7 | Proposed model for TrxA binding and toxicity of TreX. a Structural comparison of the TrxA (purple) binding to its substrate PAPS (left, PDB code: 2O8V), its client T7 polymerase (middle, PDB code: 6P7E), and TreX toxin (right). TrxA is shown in purple, PAPS in pink, T7 polymerase in cyan, DNA in gray, TreX in red, and TriX in green. **b** Model of secretion of TreX (red), activation by TrxA (purple), and growth inhibition by ADP-ribosylation of FtsZ (blue).

Discussion

Secreted bacterial toxins generally act autonomously on their targets. Here we report that TrxA acts as a chaperone for the *X. bovienii* Rhs toxin TreX. Only a few cases documented the requirement of cellular proteins for the activity of secreted toxins. For example, the elongation factor EF-Tu and the O-acetylserine sulfhydrylase CysK have been shown to interact with and support the activity of 2 tRNAse toxic domains, CdiA-CT^{EC869} and CdiA-CT^{EC536}, that are secreted by CDI systems encoded by different pathogenic *E. coli* strains[65–68]. Here, we have shown that the *X. bovienii* Rhs ADP-ribosyltransferase toxin TreX requires the reduced form of TrxA for its activity. Surprisingly, TreX lacks cysteines and thus cannot be a redox substrate of TrxA. Instead, we have found that the TrxA-TreX complex forms the active functional unit that ADP-ribosylates the essential septum protein FtsZ to inhibit bacterial cell division (Fig. 7b). The crystal structure revealed that TrxA binds to the C-terminal extension of TreX, which is located away from the active site. This leaves the active site free to interact with and ADP-ribosylate its target FtsZ. Bacteria from the same species are protected by the presence of the TriX immunity protein that neutralizes the toxin forming a TrxA-TreX-TriX ternary complex, in which TriX occludes the active site of TreX. Interestingly, such an architecture has been observed in the case of the CdiA-CT^{EC536} toxin and its partners. While CysK interacts with the C-terminal extension of the CdiA-CT^{EC536} toxin to stabilize it, the immunity protein interacts exclusively with the CdiA-CT^{EC536} nuclease active site[66]. In another reported case, the CdiA-CT^{EC869} secreted toxin is dependent on helper protein EF-Tu to recognize the substrate aatRNAs[65]. In yet another case, the EF-Tu is required for delivery of T6SS secreted *Pseudomonas aeruginosa* Tse6 toxin into recipient cells[69].

More generally, secreted toxins are usually intrinsically dependent on the interaction with other proteins, such as the secretion machinery or target cell receptors. In addition, many secreted toxins are likely to require unfolding during transport and refolding when they reach the targeted compartment in the target cell i.e., periplasm or cytoplasm in the case of Gram-negative bacteria. For example, translocation of Colicin M, which acts in the periplasm of prey cells, has be shown to be dependent on the FkpA peptidyl prolyl cis/trans isomerase (PPIase)[70,71]. Toxins that target eukaryotic cells may have to cross several membranes to reach the targeted compartment. For example, the enzymatic subunits of binary ADP-ribosylating toxins from *Clostridia* depend on the host PPIases for translocation and refolding[72,73]. Host PPIases from the Cyp family as well as the Hsp90 and Hsp70 chaperones have also been shown to be required for the activity of the *Bordetella* pertussis toxin[74]. While the TreX toxin is the first example of a target-cell chaperone-dependent Rhs toxin, little is known about the translocation of toxins from this family. We and others have reported that Rhs is a molecular cocoon encapsulating the C-terminal toxic domain[19,20]. Upon secretion, the cocoon is autocleaved, priming it for toxin release, but how exactly the toxin reaches the cytoplasm of the target cell and how it is extracted from the cocoon remains to be investigated. Structural studies have shown that the toxic domains when inside the cocoons might reside in a partially unfolded state[19,20]. In the structurally related family of Rhs-repeat proteins Tc toxins, the toxic domain is indeed extracted from the cocoon in its unfolded state[75]. The Rhs-fold cocoon therefore likely provides stability and protection for toxic domains during the initial steps of translocation, however it might further impose a (re)folding step needed for (or after) the extraction of the toxin[75]. It is therefore likely that other Rhs toxins also require cellular chaperones to adopt the active fold once reaching the targeted cellular compartment. However, TrxA is certainly not a universal chaperone of Rhs toxins or ADP-ribosyltransferases, since previously described ART toxins were active in vitro independently of TrxA.

Chaperone proteins bind their clients in their unfolded states typically protecting their hydrophobic regions from aggregation and allowing them to adopt proper 3D structure. While most ternary structures of proteins are the result of transient non-covalent interactions, a specific case is the formation of covalent disulfide bonds that involves the thiol groups of two cysteines. Due to their reversible nature, the formation of disulfide bonds in proteins can act as molecular switch that regulates protein activity. Therefore, oxidoreductases, like chaperones assist proteins in obtaining their active conformation, as they control the redox state of disulfide bonds and therefore a change in protein folding. Notably, the entry of bacterial toxins such as cholera, antrax, diphteria or botulinum relies on the oxidation or reduction of specific disulfide bonds of the toxins or of the host receptors[36–39].

In this study, we showed that the TreX toxin is an ADP-ribosyltransferase distantly related to previously characterized Scabin and ScARP toxins produced by *Streptomyces*. Scabin was shown to be stabilized by two disulfide bridges formed in its N-terminal and C-terminal regions[40]. TreX is part of the polymorphic Rhs protein, but the toxic domain itself is shorter than Scabin and lacks the N-terminal part but retains a structurally similar C-terminal extension. TreX does not possess cysteine residues, however its C-terminal extension binds to the active site of reduced TrxA. Our data showed that TreX depends on TrxA for structural stabilization and activity as TreX is mostly insoluble in the absence of TrxA. It has been previously reported that TrxA associates with the phage T7 DNA polymerase without any redox reaction, via specific poorly structured loop, to serve as a processivity factor[76]. In addition, TrxA is essential for infection of many phages (Podoviruses and Myoviruses) for the same functional reason[77,78]. Interestingly, it has been recently demonstrated that the *Salmonella* thioredoxin acts as a chaperone for structurally diverse response regulators important in virulence, independently of its oxidoreductase activity[60,61]. While previous studies have recognized the moonlighting activity of TrxA as a chaperone, it remained unclear how such function could have evolved. In this work, we provide a case study which suggests that chaperone clients of TrxA have most likely evolved from ancestral redox substrates. As a result, the active site of TrxA appears to be universally used for redox substrates as well as chaperone-clients.

Methods

Bioinformatic analyses

Rhs were detected by blast homology search using amino acid sequences of previously detected Rhs proteins (plu0353, plu3120, plu4280) from *Photorhabdus laumondii* TTO1 (taxid: 2218628)[18] as query against the *X. bovienii* SS-2004 genome (taxid: 406818)[27]. Rhs toxic domains were identified by manually searching for the DPxGL motives in the C-terminal part of the protein sequence. The C-terminal toxin sequences were then screened for conserved domains using jackhmmer database (EMBL-EBI), their structures were predicted using AlphaFold2 (ColabFold v1.5.5)[63] and the resulting models were searched for homologs against the DALI server[79]. Structural alignments were performed and visualized using ChimeraX program[80]. Phylogenetic trees were analyzed with iTOL v 6.9.1[81].

Plasmid construction

Rhs C-terminal toxin domains were amplified from the *X. bovienii* SS-2004 genomic DNA using oligonucleotides indicated in the Supplementary Table 1. To add the Shine-Dalgarno sequence and C-terminal flag-tag, the pBAD33 vector was amplified with oligonucleotides F-pBAD-Sal-flag and R-pBAD-sd-sac. Toxic domains were then cloned into the amplified pBAD33 vector through the SacI and SalI restriction sites. For further in vivo experiments, the *treX* toxin gene and *triX* immunity gene were cloned into the pBAD33 and pKK223-3 vectors via the XbaI/PstI and EcoRI/PstI restriction sites respectively, from the synthetic DNA fragments with codon-optimized sequences (IDT DNA technology). Rhs C-terminal toxin from $treX_{Pm}$ was cloned from *P. moraviensis* R28-S genome and *S. proteamaculans* Tre1 toxin and Tri1 immunity were cloned from synthetic genes (sequences provided in Supplementary Table 1). All *treX* as well as *trxA* mutations were generated by PCR amplification with mutation-bearing oligonucleotides (Supplementary Table 1). PCR products were then phosphorylated and ligated before transformation.

For bacterial double hybrid assays, *treX* was amplified using oligonucleotides listed in Supplementary Table 1 and cloned in frame with the T18 domain of the *Bordetella pertussis* adenylate cyclase in the pUT18C vector via the PstI and EcoRI restriction sites. The *triX* was cloned in frame with the T25 domain of adenylate cyclase in the pKT25 plasmid via PstI/EcoRI restriction sites or in the pKNT plasmid via HindIII/EcoRI restriction sites, as for the N- or C-terminal fusion respectively.

For the construction of pCH10163-Cdi::*treX-triX* chimera, the translocation domain (starting at the VENN motif) of the orphan 11 of the *E. coli* EC869 was amplified from the pCH10175 plasmid. The *treX-triX* gene pair was amplified from the genomic DNA of *X. bovienii* SS-2004 strain using the oligonucleotides provided in the Supplementary Table 1. The two fragments were then assembled by a joint-PCR and by further joint-PCR fused with 500 bp recombination fragments identical to upstream and downstream regions of the pCH10163 plasmid. Linearized pCH10163 plasmid (SphI digestion) and joint-PCR generated fragment were purified and co-electroporated into MG1655 cells expressing the lambda red recombineering system. Cells carrying the recombinant plasmid were selected on YEG-agar supplemented with 20 µg/mL chloramphenicol and 10 mM D/L-p-chlorophenylalanine.

For construction of his-TEV-fused TrxA, the *trxA* genes were amplified from *E. coli* MG1655 or from *X. bovienii* SS-2004 genomic

DNA and cloned into the pETduet vector amplified with oligonucleotides adding the TEV cleavage site followed by the BmtI restriction site. Cloning was performed using BmtI and HindIII restriction sites.

To generate pCDF-TreX_E102A, the mutated *treX* gene was amplified from the pBAD33-TreX_E102A plasmid using oligonucleotides provided in Table S1. To generate the pCDF-*treX-triX*-strep and pRSF-*triX*-strep constructs, genes were amplified from *X. bovienii* SS-2004 genomic DNA. The pCDF-duet and pRSF-duet vectors were amplified with F-duet-strep-sal and R-duet-sac oligonucleotides adding the C-terminal strep tag separated by the SalI restriction site. Genes were then cloned through SacI/SalI restriction sites.

The *E. coli* MG1655 *ftsZ* gene was cloned through BmtI/HindIII sites into pETduet plasmid derivative carrying N-terminal 6xhis-tagged SUMO protein followed by the TEV protease cleavage site. The *E. coli* MG1655 *trxB* gene was cloned through HindIII/BmtI sites into the pETduet plasmid amplified with F-duet-Bmt-his and R-duet-Hind oligonucleotides adding the C-terminal 6x his tag.

All genes were amplified using the Q5 DNA polymerase, digested with respective restriction enzymes and ligated with T4 DNA ligase. All molecular biology reagents were purchased from NEB and used according to manufacturer's instructions. All constructs were verified by sequencing (Eurofins) of purified plasmids.

In vivo toxicity assays

In vivo toxicity assays were performed in the *E. coli* DJ624 Δ*ara* strain or in MC4100 or its derivatives when indicated. Strains were transformed with pBAD33 vectors carrying gene Rhs toxic domains, wild-type or mutant versions of *treX* or empty cloning vectors for control, and/or pKK223-3 vector carrying *triX* antitoxin gene. Overnight cultures were adjusted to identical OD_{600nm} and 10-fold dilution series were performed in 10 mM $MgSO_4$. Ten µl were spotted on LB agar plates supplemented either with 1% of glucose or 0.2% of arabinose and 1 mM of IPTG as indicated and appropriate antibiotics. Plates were imaged after incubation at 37 °C for 18 h.

Bacterial two-hybrid assays

Pairs of pKT25 and pUT18C plasmid derivatives where T18 or T25 domains of adenylate cyclase are fused with TreX or TriX were then transformed in the *E. coli* BTH101 strain. Overnight cultures of each strain were started on M9 minimal media supplemented with appropriate antibiotics and 1% of glucose. Ten µl of overnight cultures were spotted on M9 medium plates supplemented with 1% glucose, 0.5 mM IPTG, 40 µg/m Xgal, and appropriate antibiotics. Plates were then incubated at 37 °C for 18 h before imaging. Empty vectors where used as negative controls and plasmids carrying T18::zip and T25::zip (leucine zipper region of the yeast GCN4 protein) fusions were used as a positive control.

Microscopy

E. coli DJ624 Δ*ara* strains carrying pBAD33-*treX* and pKK22-3-3-*triX* when indicated were grown in M9 media supplemented with 1% of glucose and appropriate antibiotics. At OD_{600nm} around 0.2, cells were washed and resuspended in fresh M9 medium supplemented with 0.2% arabinose and 1 mM IPTG. Four µl samples were taken at different time points after induction and spotted on poly-L-lysine coated glass slides.

For the bacterial competition experiments, an *E. coli* MG1655 pUA66-pR2U-GFP*mut2* strain was transformed with the pCH10163-Cdi::TreX-TriX chimera described above. *E. coli* MG1655 Nal^R PT5-mCherry strain was used as a target cell and was transformed with either the empty pKK223-3 vector or the pKK223-3-TriX. Strains were grown to an OD_{600nm} of around 0.2, washed, resuspended in fresh LB medium and supplemented with 1 mM IPTG without antibiotics, and mixed in a 1:1 ratio. Aliquots of cell mixture were taken every hour, stained with 1 µg/ml DAPI for 15 min on ice, in the dark, and then plated on agarose LB pads. Pictures at different wavelengths were taken using an inverted microscope Zeiss Axio Observer equipped with a 100x oil-immersion objective, 120 V HXP lamp, and Hamamatsu ORCA-Flash 4.0 digital camera. Pictures in different fluorescence channels were merged with the Zeiss ZEN 3.2 (blue edition) software.

Selection and sequencing of TreX-resistant mutants

To select for TreX-resistant mutants, TreX was first induced in the *E. coli* DJ624 Δ*ara* strain from the pBAD33-*treX* plasmid. Resistant mutants were selected on solid LB agar plates supplemented with 0.2% arabinose. 48% of independent cultures gave resistant colonies, with the average frequency of ~1.1×10^{-6}. To reduce the number of false positives (e.g., mutants defective for toxin expression), the mutants were challenged with the *E. coli* MG1655 expressing the chimeric Cdi:TreX-TriX system from pCH10163-Cdi::*treX-triX*. *E. coli* DJ624 Δ*ara* pBAD33-*treX* mutants that maintain a stable ratio during the competition with the *E. coli* MG1655 pCH10163-Cdi::*treX-triX* were selected. Only ~5% of colonies showed resistance to the Cdi::*treX-triX* attack. Five independent TreX-resistant mutants were sent for Illumina-whole genome sequencing (Eurofins Genomics).

In vitro ADP-ribosylation assays

Wild-type TreX toxin was produced in vitro in PURExpress coupled transcription-translation reaction from a DNA fragment amplified using 5-UTR-TreX and 3-UTR-TreX oligonucleotides.

For ADP-ribosylation on the crude cellular extract, the *E. coli* MG1655 strain was grown to OD_{600nm} of around 0.5, concentrated 20 times by centrifugation and resuspended into 50 mM Tris-HCl pH 8, 150 mM NaCl, 1 mM TCEP buffer. When indicated, final concentration of 0.1 mM 6-biotin-17-NAD^+ and 1 µL of in vitro produced TreX toxin were added into 10 µL suspension of sonicated cells and incubated for 30 min at 37 °C.

All in vitro ADP-ribosylation reactions were performed in 10 µL reactions that contained 10 µM of purified tagless FtsZ protein and 0.1 mM 6-biotin-17-NAD^+. When indicated, the reactions also contained 1 µL of in vitro synthesized TreX toxin, 1 mM DTT, 1 µM of wild-type or mutated TrxA-his, 1 µM of TrxB-his, 1 mM NADPH, 10 µM of TriX immunity protein. ADP-ribosylation with purified TreX-TrxA complex contained different concentrations of complex, that was purified as described in protein expression and purification section.

ADP-ribosylation reactions were incubated for 15 or 30 min at 37 °C as indicated in figure legends. Reactions were then separated using 15% SDS-PAGE and transferred on nitrocellulose membranes. Membranes were stained with Ponceau to confirm equal loading and transfer, washed with water, and blocked with 3% BSA/PBS solution for 1 h. Biotin-ADPr adducts were then detected by incubating the membrane for 1 h with Streptavidin-Alkaline Phosphatase Conjugate (Invitrogen, Cat# S921) diluted 10,000-fold in 3% BSA/PBS solution. Membranes were then washed 3 times with PBS buffer and signal was detected with the fresh NBT/BCIP mixture in 100 mM Tris-HCl pH 9.5, 100 mM NaCl, 10 mM $MgCl_2$ buffer.

Protein interaction (pull-down) assays

The *E. coli* BL21 (DE3) strain was (co)transformed with pET28b-*trxA*-his, pCDF-*treX*_E102A-strep plasmids or their derivatives. Protein production was induced in 50 mL bacterial cultures in liquid LB medium with 1 mM IPTG at OD_{600nm} of around 0.8. Induction continued overnight at 16 °C. Cells were then collected by centrifugation at 5000 × *g* and resuspended in cold 100 mM Tris-HCl pH 8, 250 mM NaCl, 1 mM TCEP buffer and sonicated 3 times for 1 min with 1 s pulses on ice. Protein extracts were collected after centrifugation for 45 min at 20,000 × *g*. Extracts were then loaded on Strep-Tactin Superflow resin (IBA Technology) or TALON resin (Takara Bio) for strep- or his- pull-down respectively. Protein extracts were incubated with resin beads for 1 h at 4 °C with gentle rocking. Resin was then collected by centrifugation

and washed with 20 column volumes (CV) of protein resuspension buffer. Proteins were eluted with 2 CV of elution buffer that consisted of protein resuspension buffer supplemented with either 5 mM desthiobiotin for strep- or with 200 mM imidazole pH8 for his- pull-down purifications respectively. Aliquots of 1 µL of protein extract and 10 µL of elution fractions were loaded on 15% SDS-PAGE gel, migrated for 1 h at 200 V. Proteins were detected by Coomassie staining, or transferred onto nitrocellulose membrane and analyzed by Western-blot. Commercial monoclonal anti-his-tag (Proteintech Cat# 66005-1-Ig, dilution 1:5000) and anti-strep-tag (BioRad Cat# MCA2489, dilution 1: 1000) antibodies were used for Western-blot, followed by a secondary antibody coupled to alkaline phosphatase (Millipore Cat# AP503A, dilution 1: 5000) and detection by NBT/BCIP as described above.

Large scale protein expression and purification

Production of his-SUMO-FtsZ, TrxB-his, TriX-strep, TreX-TriX-strep, his-TEV-TrxA (*E. coli* and *X. bovienii* version), and his-TEV-TrxA co-production with TreX_E102A-strep, was induced from plasmids listed in Supplementary Table 2 in *E. coli* BL21 (DE3) strain. Proteins from two-to-four-liter bacterial cultures were purified as described in previous section, except that larger volumes of protein purification resins were used for purification in gravity protein purification columns. Protein binding was followed by 5 wash steps with 5 CV of protein resuspension buffer and then 3 elution fractions of 1 mL with corresponding his- or strep- elution buffers.

After the affinity chromatography, histidine tag from TrxA protein and his-SUMO tag from FtsZ protein were removed by incubation of elution fractions with TEV protease at 30 °C. Complete tag removal was confirmed by SDS-PAGE analysis. All purified proteins were then subjected to a second step of purification by size-exclusion chromatography on Superdex 75 10/300 column (Cytiva) equilibrated with 50 mM Tris-HCl pH8, 250 mM NaCl, 1 mM TCEP buffer. Column was calibrated using Gel Filtration Standard (Bio-Rad). For crystallography and molecular weight analyses, the TreX-TriX-TrxA complex was formed by incubating the tagless TreX protein and TreX-TriX-strep complex purified separately for 1 h before gel filtration.

For purification of FtsZ, TrxA, TrxB, and TriX used in the in vitro ADP-ribosylation assays, size exclusion chromatography was performed in 50 mM Tris-HCl pH8, 250 mM NaCl buffer without reducing agents.

For the ADP-ribosylation assays using the preformed TreX-TrxA complex, wild-type TreX toxin was separated from TreX-TriX-strep complex in denaturing conditions and refolded in presence of excess of TrxA and 1 mM DTT. The TreX-TrxA complex was further separated from free TrxA and DTT, and eluted into 50 mM Tris-HCl, 150 mM NaCl buffer using size exclusion chromatography with Superdex 75 10/300 column. The purified complex was then concentrated using Amicon Ultra centrifugal filter.

Crystallization, data collection and structural determination

Purified TreX-TriX and TreX-TriX-TrxA protein complexes were concentrated to 15–25 mg · mL^{-1} and screened for crystal formation in Swissci 96-well 2-drop MRC crystallization plates (Molecular Dimensions) using commercial precipitation solutions: LMB, JCSGplus, PactPremier, MembFac (Molecular Dimensions) or Crystal Screen (Hampton Research). For the TreX-TriX complex, diffraction quality crystals were obtained in 1.1 M Sodium malonate dibasic monohydrate, 0.1 M HEPES pH 7.0, 0.5% v/v Jeffamine ED-2003 (JCSGplus kit). For the ternary TreX-TriX-TrxA complex, crystals were obtained in 0.2 M Ammonium sulfate, 0.02 M Sodium chloride, 0.02 M Sodium acetate pH 4.0, 33% v/v PEG 200 (MemGold kit). For TreX-TriX-TrxA$_{Xb}$ complex, crystals were obtained in 0.2 M Calcium chloride dihydrate, 0.1 M Tris-HCl pH 8.0, 44% v/v PEG 400. Before freezing in liquid nitrogen, crystals were cryo-protected by quick immersion into the well solution supplemented with 20% glycerol or 20% PEG400 for binary and for ternary complex crystals, respectively. TreX-TriX-TrxA$_{Xb}$ complex were frozen without additional cryo-protecting solution. Diffraction data was collected at SOLEIL Synchrotron (Gif-sur-Yvette, Paris, France) at the PROXIMA-2A beamline. All crystal diffraction data was collected at 100 °K at 0.82656 Å wavelength (for TreX-TriX complex) or at 0.97856 Å (for the TreX-TriX-TrxA complexes).

Structures were solved by molecular replacement using AlphaFold2[63] models of TreX and TriX models and TrxA structure (PDB:2H6X) using Phaser in the Phenix package[82]. Initial models were built with Autobuild in Phenix package[82], and completed by manual building with Coot[83] and refined with Phenix[82]. Refined structures contain no Ramachandran outliers—TreX-TriX complex 97.66% Ramachandran favored, 2.34% Ramachandran allowed; TreX-TriX-TrxA 98.09% favored, 1.91% allowed, and TreX-TriX-TrxA$_{Xb}$ 97.56% favored, 2.44% allowed. Data collection and refinement statistics are provided in Supplementary Table 3.

Statistics and reproducibility

Bacterial growth inhibition, bacterial two hybrid assays and microscopy images are representative of at least three independent biological replicates. All ADP-ribosylation and protein pull-down assays were reproduced and analyzed by SDS-PAGE and western-blot at least three times. Representative images of gels and blots are shown. Evolution of TreX-resistant mutants was attempted in more than 100 independent experiments and statistics are provided in "methods" section. For each structure determination, X-ray diffraction was collected from 3 to 4 crystals independently. Data was analyzed separately and dataset yielding best resolution was further used for structure modeling and refinement.

Reporting summary

Further information on research design is available in the Nature Portfolio Reporting Summary linked to this article.

Data availability

The X-ray crystallography data generated in this study have been deposited to the Protein Data Bank (PDB) under the accession codes 8S2M (TreX-TriX complex), 8S2N (TreX-TriX-TrxA$_{Ec}$ complex), and 9GCO (TreX-TriX-TrxA$_{Xb}$ complex). An image of a portion of the electron density map for each structure is provided in Supplementary Fig. 13. Other previously reported structures used in this study are available in PDB under accession codes: 6DRH, 6VV4, 5ZJ4, 4TLV, 2O8V, 6P7E, 2H6X. Uncropped gels and blots generated in this study are provided in Source Data file. Source data are provided with this paper.

References

1. Braun, V. & Patzer, S. I. Intercellular communication by related bacterial protein toxins: colicins, contact-dependent inhibitors, and proteins exported by the type VI secretion system. *FEMS Microbiol. Lett.* **345**, 13–21 (2013).
2. Cherrak, Y., Flaugnatti, N., Durand, E., Journet, L. & Cascales, E. Structure and activity of the type VI secretion system. *Microbiol. Spectr.* **7**, 0031–2019 (2019).
3. Gallegos-Monterrosa, R. & Coulthurst, S. J. The ecological impact of a bacterial weapon: microbial interactions and the Type VI secretion system. *FEMS Microbiol. Rev.* **45**, fuab033 (2021).
4. Flaugnatti, N. et al. Structural basis for loading and inhibition of a bacterial T6SS phospholipase effector by the VgrG spike. *EMBO J.* **39**, e104129 (2020).
5. Quentin, D. et al. Mechanism of loading and translocation of type VI secretion system effector Tse6. *Nat. Microbiol.* **3**, 1142–1152 (2018).
6. Le, N.-H. et al. Peptidoglycan editing provides immunity to Acinetobacter baumannii during bacterial warfare. *Sci. Adv.* **6**, eabb5614 (2020).

7. Flaugnatti, N. et al. Human commensal gut Proteobacteria withstand type VI secretion attacks through immunity protein-independent mechanisms. *Nat. Commun.* **12**, 5751 (2021).
8. Toska, J., Ho, B. T. & Mekalanos, J. J. Exopolysaccharide protects Vibrio cholerae from exogenous attacks by the type 6 secretion system. *Proc. Natl. Acad. Sci. USA* **115**, 7997–8002 (2018).
9. Hersch, S. J. et al. Envelope stress responses defend against type six secretion system attacks independently of immunity proteins. *Nat. Microbiol.* **5**, 706–714 (2020).
10. Granato, E. T., Smith, W. P. J. & Foster, K. R. Collective protection against the type VI secretion system in bacteria. *ISME J.* **17**, 1052–1062 (2023).
11. Robitaille, S., Trus, E. & Ross, B. D. Bacterial defense against the Type VI secretion system. *Trends Microbiol.* **29**, 187–190 (2021).
12. Ruhe, Z. C., Low, D. A. & Hayes, C. S. Polymorphic toxins and their immunity proteins: diversity, evolution, and mechanisms of delivery. *Annu. Rev. Microbiol.* **74**, 497–520 (2020).
13. Jurėnas, D. & Journet, L. Activity, delivery, and diversity of Type VI secretion effectors. *Mol. Microbiol.* **115**, 383–394 (2021).
14. Suskiewicz, M. J., Prokhorova, E., Rack, J. G. M. & Ahel, I. ADP-ribosylation from molecular mechanisms to therapeutic implications. *Cell* **186**, 4475–4495 (2023).
15. Bullen, N. P. et al. An ADP-ribosyltransferase toxin kills bacterial cells by modifying structured non-coding RNAs. *Mol. Cell* **82**, 3484–3498.e11 (2022).
16. Jurėnas, D. et al. Salmonella antibacterial Rhs polymorphic toxin inhibits translation through ADP-ribosylation of EF-Tu P-loop. *Nucleic Acids Res.* **50**, 13114–13127 (2022).
17. Ting, S.-Y. et al. Bifunctional immunity proteins protect bacteria against FtsZ-Targeting ADP-Ribosylating Toxins. *Cell* **175**, 1380–1392.e14 (2018).
18. Jurėnas, D. et al. Photorhabdus antibacterial Rhs polymorphic toxin inhibits translation through ADP-ribosylation of 23S ribosomal RNA. *Nucleic Acids Res.* **49**, 8384–8395 (2021).
19. Jurėnas, D. et al. Mounting, structure and autocleavage of a type VI secretion-associated Rhs polymorphic toxin. *Nat. Commun.* **12**, 6998 (2021).
20. Günther, P. et al. Structure of a bacterial Rhs effector exported by the type VI secretion system. *PLoS Pathog.* **18**, e1010182 (2022).
21. Thomas, G. M. & Poinar, G. O. Xenorhabdus gen. nov., a genus of entomopathogenic, nematophilic bacteria of the family Enterobacteriaceae. *Int. J. Syst. Evolut. Microbiol.* **29**, 352–360 (1979).
22. Clarke, D. J. Photorhabdus: a model for the analysis of pathogenicity and mutualism. *Cell Microbiol.* **10**, 2159–2167 (2008).
23. Boemare, N. Interactions between the partners of the entomopathogenic bacterium nematode complexes, Steinernema-Xenorhabdus and Heterorhabditis-Photorhabdus. *Nematology* **4**, 601–603 (2002).
24. Goodrich-Blair, H. & Clarke, D. J. Mutualism and pathogenesis in Xenorhabdus and Photorhabdus: two roads to the same destination. *Mol. Microbiol.* **64**, 260–268 (2007).
25. Martens, E. C., Heungens, K. & Goodrich-Blair, H. Early colonization events in the mutualistic association between Steinernema carpocapsae nematodes and Xenorhabdus nematophila bacteria. *J. Bacteriol.* **185**, 3147–3154 (2003).
26. Snyder, H., Stock, S. P., Kim, S.-K., Flores-Lara, Y. & Forst, S. New insights into the colonization and release processes of Xenorhabdus nematophila and the morphology and ultrastructure of the bacterial receptacle of its nematode host, Steinernema carpocapsae. *Appl. Environ. Microbiol.* **73**, 5338–5346 (2007).
27. Chaston, J. M. et al. The entomopathogenic bacterial endosymbionts Xenorhabdus and Photorhabdus: convergent lifestyles from divergent genomes. *PLoS ONE* **6**, e27909 (2011).
28. Tobias, N. J. et al. Natural product diversity associated with the nematode symbionts Photorhabdus and Xenorhabdus. *Nat. Microbiol.* **2**, 1676–1685 (2017).
29. Akhurst, R. J. Antibiotic activity of Xenorhabdus spp., bacteria symbiotically associated with insect pathogenic nematodes of the families Heterorhabditidae and Steinernematidae. *J. Gen. Microbiol.* **128**, 3061–3065 (1982).
30. Zhou, Q. et al. Structure and biosynthesis of xenoamicins from entomopathogenic Xenorhabdus. *Chemistry* **19**, 16772–16779 (2013).
31. ffrench-Constant, R. H., Dowling, A. & Waterfield, N. R. Insecticidal toxins from Photorhabdus bacteria and their potential use in agriculture. *Toxicon* **49**, 436–451 (2007).
32. Morales-Soto, N. & Forst, S. A. The xnp1 P2-like tail synthesis gene cluster encodes xenorhabdicin and is required for interspecies competition. *J. Bacteriol.* **193**, 3624–3632 (2011).
33. Dreyer, J., Malan, A. P. & Dicks, L. M. T. Bacteria of the genus Xenorhabdus, a novel source of bioactive compounds. *Front. Microbiol.* **9**, 3177 (2018).
34. McMullen, J. G. et al. Variable virulence phenotype of Xenorhabdus bovienii (γ-Proteobacteria: Enterobacteriaceae) in the absence of their vector hosts. *Microbiology* **163**, 510–522 (2017).
35. Kochanowsky, R. M., Bradshaw, C., Forlastro, I. & Stock, S. P. Xenorhabdus bovienii strain jolietti uses a type 6 secretion system to kill closely related Xenorhabdus strains. *FEMS Microbiol. Ecol.* **96**, fiaa073 (2020).
36. Papini, E., Rappuoli, R., Murgia, M. & Montecucco, C. Cell penetration of diphtheria toxin. Reduction of the interchain disulfide bridge is the rate-limiting step of translocation in the cytosol. *J. Biol. Chem.* **268**, 1567–1574 (1993).
37. Tsai, B., Rodighiero, C., Lencer, W. I. & Rapoport, T. A. Protein disulfide isomerase acts as a redox-dependent chaperone to unfold cholera toxin. *Cell* **104**, 937–948 (2001).
38. Fischer, A. & Montal, M. Crucial role of the disulfide bridge between botulinum neurotoxin light and heavy chains in protease translocation across membranes. *J. Biol. Chem.* **282**, 29604–29611 (2007).
39. Sun, J. & Collier, R. J. Disulfide bonds in the ectodomain of anthrax toxin receptor 2 are required for the receptor-bound protective-antigen pore to function. *PLoS ONE* **5**, e10553 (2010).
40. Lyons, B. et al. Scabin, a novel DNA-acting ADP-ribosyltransferase from Streptomyces scabies. *J. Biol. Chem.* **291**, 11198–11215 (2016).
41. Hill, C. W., Sandt, C. H. & Vlazny, D. A. Rhs elements of Escherichia coli: a family of genetic composites each encoding a large mosaic protein. *Mol. Microbiol.* **12**, 865–871 (1994).
42. Poole, S. J. et al. Identification of functional toxin/immunity genes linked to contact-dependent growth inhibition (CDI) and rearrangement hotspot (Rhs) systems. *PLoS Genet.* **7**, e1002217 (2011).
43. Koskiniemi, S. et al. Rhs proteins from diverse bacteria mediate intercellular competition. *Proc. Natl. Acad. Sci. USA* **110**, 7032–7037 (2013).
44. Aravind, L., Zhang, D., de Souza, R. F., Anand, S. & Iyer, L. M. The natural history of ADP-ribosyltransferases and the ADP-ribosylation system. *Curr. Top. Microbiol. Immunol.* **384**, 3–32 (2015).
45. Han, S. & Tainer, J. A. The ARTT motif and a unified structural understanding of substrate recognition in ADP-ribosylating bacterial toxins and eukaryotic ADP-ribosyltransferases. *Int. J. Med. Microbiol.* **291**, 523–529 (2002).
46. Davies, A. H. et al. Functional significance of active site residues in the enzymatic component of the Clostridium difficile binary toxin. *Biochem. Biophys. Rep.* **8**, 55–61 (2016).
47. Barth, H., Preiss, J. C., Hofmann, F. & Aktories, K. Characterization of the catalytic site of the ADP-ribosyltransferase Clostridium botulinum C2 toxin by site-directed mutagenesis. *J. Biol. Chem.* **273**, 29506–29511 (1998).

48. Tsurumura, T. et al. Arginine ADP-ribosylation mechanism based on structural snapshots of iota-toxin and actin complex. *Proc. Natl. Acad. Sci. USA* **110**, 4267–4272 (2013).
49. Vatta, M., Lyons, B., Heney, K. A., Lidster, T. & Merrill, A. R. Mapping the DNA-binding motif of Scabin Toxin, a guanine modifying enzyme from Streptomyces scabies. *Toxins* **13**, 55 (2021).
50. Yoshida, T. & Tsuge, H. Substrate N2 atom recognition mechanism in pierisin family DNA-targeting, guanine-specific ADP-ribosyltransferase ScARP. *J. Biol. Chem.* **293**, 13768–13774 (2018).
51. Becker, A. et al. Structure of CARDS toxin, a unique ADP-ribosylating and vacuolating cytotoxin from Mycoplasma pneumoniae. *Proc. Natl. Acad. Sci. USA* **112**, 5165–5170 (2015).
52. Bose, S. et al. ADP-ribosylation of NLRP3 by Mycoplasma pneumoniae CARDS toxin regulates inflammasome activity. *mBio* **5**, e02186–14 (2014).
53. Aoki, S. K. et al. Contact-dependent inhibition of growth in Escherichia coli. *Science* **309**, 1245–1248 (2005).
54. Hayes, C. S., Aoki, S. K. & Low, D. A. Bacterial contact-dependent delivery systems. *Annu. Rev. Genet.* **44**, 71–90 (2010).
55. Morse, R. P. et al. Structural basis of toxicity and immunity in contact-dependent growth inhibition (CDI) systems. *Proc. Natl. Acad. Sci. USA* **109**, 21480–21485 (2012).
56. Carvalho, A. P., Fernandes, P. A. & Ramos, M. J. Similarities and differences in the thioredoxin superfamily. *Prog. Biophys. Mol. Biol.* **91**, 229–248 (2006).
57. Bittner, L.-M., Arends, J. & Narberhaus, F. When, how and why? Regulated proteolysis by the essential FtsH protease in Escherichia coli. *Biol. Chem.* **398**, 625–635 (2017).
58. Qiao, Z. et al. Cryo-EM structure of the entire FtsH-HflKC AAA protease complex. *Cell Rep.* **39**, 110890 (2022).
59. Stewart, E. J., Aslund, F. & Beckwith, J. Disulfide bond formation in the Escherichia coli cytoplasm: an in vivo role reversal for the thioredoxins. *EMBO J.* **17**, 5543–5550 (1998).
60. Kim, J.-S. et al. Promiscuity of response regulators for thioredoxin steers bacterial virulence. *Nat. Commun.* **13**, 6210 (2022).
61. Song, M., Kim, J.-S., Liu, L., Husain, M. & Vázquez-Torres, A. Antioxidant defense by thioredoxin can occur independently of canonical thiol-disulfide oxidoreductase enzymatic activity. *Cell Rep.* **14**, 2901–2911 (2016).
62. Huber, H. E., Tabor, S. & Richardson, C. C. Escherichia coli thioredoxin stabilizes complexes of bacteriophage T7 DNA polymerase and primed templates. *J. Biol. Chem.* **262**, 16224–16232 (1987).
63. Mirdita, M. et al. ColabFold: making protein folding accessible to all. *Nat. Methods* **19**, 679–682 (2022).
64. Doublié, S., Tabor, S., Long, A. M., Richardson, C. C. & Ellenberger, T. Crystal structure of a bacteriophage T7 DNA replication complex at 2.2 A resolution. *Nature* **391**, 251–258 (1998).
65. Jones, A. M., Garza-Sánchez, F., So, J., Hayes, C. S. & Low, D. A. Activation of contact-dependent antibacterial tRNase toxins by translation elongation factors. *Proc. Natl. Acad. Sci. USA* **114**, E1951–E1957 (2017).
66. Johnson, P. M. et al. Unraveling the essential role of CysK in CDI toxin activation. *Proc. Natl. Acad. Sci. USA* **113**, 9792–9797 (2016).
67. Diner, E. J., Beck, C. M., Webb, J. S., Low, D. A. & Hayes, C. S. Identification of a target cell permissive factor required for contact-dependent growth inhibition (CDI). *Genes Dev.* **26**, 515–525 (2012).
68. Michalska, K. et al. Structure of a novel antibacterial toxin that exploits elongation factor Tu to cleave specific transfer RNAs. *Nucleic Acids Res.* **45**, 10306–10320 (2017).
69. Whitney, J. C. et al. An interbacterial NAD(P)(+) glycohydrolase toxin requires elongation factor Tu for delivery to target cells. *Cell* **163**, 607–619 (2015).
70. Hullmann, J., Patzer, S. I., Römer, C., Hantke, K. & Braun, V. Periplasmic chaperone FkpA is essential for imported colicin M toxicity. *Mol. Microbiol.* **69**, 926–937 (2008).
71. Barnéoud-Arnoulet, A. et al. Toxicity of the colicin M catalytic domain exported to the periplasm is FkpA independent. *J. Bacteriol.* **192**, 5212–5219 (2010).
72. Ernst, K., Schnell, L. & Barth, H. Host cell chaperones Hsp70/Hsp90 and peptidyl-prolyl cis/trans isomerases are required for the membrane translocation of bacterial ADP-ribosylating toxins. *Curr. Top. Microbiol. Immunol.* **406**, 163–198 (2017).
73. Ernst, K. Requirement of Peptidyl-Prolyl Cis/Trans isomerases and chaperones for cellular uptake of bacterial AB-type toxins. *Front. Cell Infect. Microbiol.* **12**, 938015 (2022).
74. Ernst, K. et al. Pharmacological targeting of host chaperones protects from pertussis toxin in vitro and in vivo. *Sci. Rep.* **11**, 5429 (2021).
75. Gatsogiannis, C. et al. Tc toxin activation requires unfolding and refolding of a β-propeller. *Nature* **563**, 209–213 (2018).
76. Hamdan, S. M. et al. A unique loop in T7 DNA polymerase mediates the binding of helicase-primase, DNA binding protein, and processivity factor. *Proc. Natl. Acad. Sci. USA* **102**, 5096–5101 (2005).
77. Qimron, U., Marintcheva, B., Tabor, S. & Richardson, C. C. Genomewide screens for Escherichia coli genes affecting growth of T7 bacteriophage. *Proc. Natl. Acad. Sci. USA* **103**, 19039–19044 (2006).
78. Šimoliūnienė, M., Kazlauskas, D., Zajančkauskaitė, A., Meškys, R. & Truncaitė, L. Escherichia coli trxAgene as a molecular marker for genome engineering of felixounoviruses. *Biochim. Biophys. Acta Gen. Subj.* **1865**, 129967 (2021).
79. Holm, L. Using Dali for protein structure comparison. *Methods Mol. Biol.* **2112**, 29–42 (2020).
80. Goddard, T. D. et al. UCSF ChimeraX: meeting modern challenges in visualization and analysis. *Protein Sci.* **27**, 14–25 (2018).
81. Letunic, I. & Bork, P. Interactive Tree of Life (iTOL) v6: recent updates to the phylogenetic tree display and annotation tool. *Nucleic Acids Res.* **52**, W78–W82 (2024).
82. Liebschner, D. et al. Macromolecular structure determination using X-rays, neutrons and electrons: recent developments in Phenix. *Acta Crystallogr. D. Struct. Biol.* **75**, 861–877 (2019).
83. Emsley, P., Lohkamp, B., Scott, W. G. & Cowtan, K. Features and development of Coot. *Acta Crystallogr. D. Biol. Crystallogr.* **66**, 486–501 (2010).

Acknowledgements

This work was supported by the European Society of Clinical Microbiology and Infectious Diseases (ESCMID Research Grant 2022 to D.J.); the Fonds National de Recherche Scientifique (FNRS-MIS F4526.23, and J.0115.24F to D.J.); FRFS-WELBIO (STG-X.251 to D.J), Internationale Brachet Stiftung (to L.V.M.); Walloon Region (ALGOTECH, 1510598 to L.V.M.); D.J. was supported by FRM post-doctoral fellowship (SPF201809007142). B.D. was supported by a PhD fellowship from the Fonds National de Recherche Scientifique FNRS-ASPIRANT. Authors would like thank to J.F. Collet (UCL, de Duve Institute) for *trxA* and *trxB* mutant strains as well as for discussions and advice throughout the project, to C. Hayes and D. Low (UC Santa Barbara, MCDB) for the plasmid encoding the CDI system, to G. Mazzucchelli (ULiege, Laboratoire de spectrométrie de masse) and P. Mansuelle (CNRS, IMM, Proteomic facility) for mass spectrometry analyses and to the staff of SOLEIL Synchrotron Proxima2 beamline for beamline allocation and assistance during data acquisition.

Author contributions

D.J. and L.V.M. designed the research. B.D., D.J., E.C., and L.T. performed research. L.V.M., E.C., L.T., and D.J. provided tools. D.J., L.V.M., and L.T.

analyzed the data. D.J. and L.V.M wrote the manuscript with contributions from all the authors. All authors approved the final revision of the manuscript.

Competing interests
The authors declare no competing interests.

Additional information
Supplementary information The online version contains supplementary material available at https://doi.org/10.1038/s41467-024-54892-w.

Correspondence and requests for materials should be addressed to Laurence Van Melderen or Dukas Jurėnas.

Peer review information *Nature Communications* thanks the anonymous reviewers for their contribution to the peer review of this work. A peer review file is available.